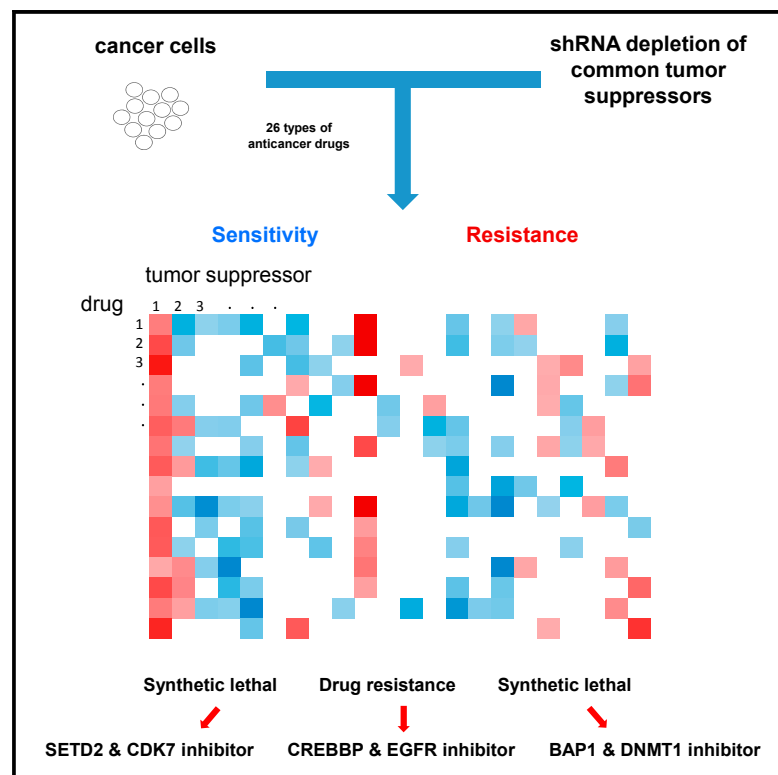


# Cell Reports

## Systematic Analysis of Drug Vulnerabilities Conferred by Tumor Suppressor Loss

### Graphical Abstract



### Authors

Hongyu Ding, Jie Zhao, Yanli Zhang, ..., Zhengjin He, Shishuang Chen, Hai Jiang

### Correspondence

hai@sibcb.ac.cn

### In Brief

Ding et al. describe how deficiencies of tumor suppressors affect cellular sensitivities to 26 types of anticancer drugs. The study reveals tumor suppressor-drug interactions potentially useful for cancer therapy.

### Highlights

- A heatmap describing drug sensitivities conferred by tumor suppressor loss
- SETD2 deficiency sensitized cells to CDK7 inhibitor
- CREBBP deficiency conferred resistance to EGFR inhibitors
- BAP1 loss sensitized cells to DNMT1 inhibitors



# Systematic Analysis of Drug Vulnerabilities Conferred by Tumor Suppressor Loss

Hongyu Ding,<sup>1,2</sup> Jie Zhao,<sup>1,2</sup> Yanli Zhang,<sup>1</sup> Jiao Yu,<sup>1</sup> Mingxian Liu,<sup>1</sup> Xiaoxi Li,<sup>1</sup> Liang Xu,<sup>1</sup> Minghui Lin,<sup>1</sup> Chuan Liu,<sup>1</sup> Zhengjin He,<sup>1</sup> Shishuang Chen,<sup>1</sup> and Hai Jiang<sup>1,3,\*</sup>

<sup>1</sup>State Key Laboratory of Cell Biology, Key Laboratory of Systems Biology, Innovation Center for Cell Signaling Network, CAS Center for Excellence in Molecular Cell Science, Shanghai Institute of Biochemistry and Cell Biology, Chinese Academy of Sciences, University of Chinese Academy of Sciences, 320 Yueyang Road, Shanghai 200031, China

<sup>2</sup>These authors contributed equally

<sup>3</sup>Lead Contact

\*Correspondence: [hai@sibcb.ac.cn](mailto:hai@sibcb.ac.cn)

<https://doi.org/10.1016/j.celrep.2019.05.043>

## SUMMARY

In addition to oncogene inhibition, targeting tumor suppressor deficiency could provide potential venues for precision cancer medicine. However, the full spectrum of drug vulnerability conferred by tumor suppressor loss remains unclear. We systematically analyzed how loss of 59 common tumor suppressors each affected cellular sensitivity to 26 different types of anticancer therapeutics. The experiments were performed in a one-gene, one-drug manner, and through such a large gene-drug iteration study, we were able to generate a drug sensitivity map that describes numerous examples of drug resistance or hypersensitivity conferred by tumor suppressor loss. We further delineated the mechanisms of several gene-drug interactions, showing that loss of tumor suppressors could modify drug sensitivity at various steps of drug action. This systematic drug sensitivity map highlights potential drug vulnerabilities associated with tumor suppressor loss, which may help expand precision cancer medicine on the basis of tumor suppressor status.

## INTRODUCTION

Inhibition of oncogenes is a major venue of current precision cancer medicine, and recent data suggest that its benefits are limited to a small portion of cancer patients (Hunter, 2016; Prasad, 2016). In contrast, tumor suppressor deficiency remains an underexplored area in precision cancer medicine. Knowledge of drug sensitivity associated with tumor suppressor loss could potentially expand therapeutic approaches for cancer, given the prevalence of tumor suppressor deficiencies in cancer.

Considering tumor suppressors' important roles in crucial cellular events, deficiencies in tumor suppressors may alter certain cellular processes, which could result in increased sensitivity to certain drugs. For example, BRCA1/2-deficient tumors are hypersensitive to PARP inhibitors (Bryant et al., 2005; Farmer et al., 2005; Tan et al., 2008). Given that there are more than 60 tumor suppressors in the COSMIC Cancer Gene Census ([\[cancer.sanger.ac.uk/census\]\(https://cancer.sanger.ac.uk/census\)\) \(Futreal et al., 2004\) and more than 20 major types of anticancer mechanisms, it is possible that loss of other tumor suppressors could sensitize cancer cells to certain drugs, thereby providing new angles to specifically attack cancer. Recently, genome-wide RNAi and CRISPR screening have been applied to study resistance mechanisms to several anticancer drugs such as 6-TG, etoposide, and BRAF inhibitor \(Koike-Yusa et al., 2014; Shalem et al., 2014; Takase et al., 2017; Wang et al., 2014; Zhu et al., 2019\). However, with a few exceptions, the full spectrum of drug vulnerabilities associated with tumor suppressor loss remains largely unknown.](https://</a></p></div><div data-bbox=)

Currently, cancer cell line comparison-based studies are used to search for novel gene-drug interactions. In such approaches, the genetic and transcriptional landscapes are determined for a large collection of cancer cell lines. In addition, sensitivities to different anticancer compounds are recorded for each cell line. On the basis of comparison of cell lines' genetic, transcriptional landscapes and their drug sensitivity profiles, gene-drug associations are predicted (Barretina et al., 2012; Garnett et al., 2012). However, a subsequent study pointed to the data inconsistency between such studies (Haibe-Kains et al., 2013). Currently, the Genomics of Drug Sensitivity in Cancer (GDSC) database provides the most comprehensive results of cell line comparison-based studies (Garnett et al., 2012; Iorio et al., 2016; Yang et al., 2013). Query of this database showed that with regard to tumor suppressors, only a limited number of gene-drug associations could be identified by such an approach (Table S1), mostly showing p53 deficiency, rendering cells resistant to drugs. Importantly, such cell line comparison-based approach could not show BRCA1/2-deficient cells are more sensitive to PARP inhibitors (Table S2). Inquiry about other well-established tumor suppressor-drug interactions further showed that cell line comparison-based approach could recapitulate only a small fraction of such interactions (Table S3).

Several aspects of the cell line comparison-based approach may have caused poor resolution on tumor suppressor-drug interactions. Cancer cell lines are vastly different from one another, which may introduce too many variables that potentially affect drug sensitivity. Analysis of the cancer cell lines used in the GDSC studies (Forbes et al., 2015) suggests that between any pair of cancer cell lines, there are several thousand genes differentially affected by mutations, copy number variations, or aberrant expression (Figure 1A). Under such a scenario, genes



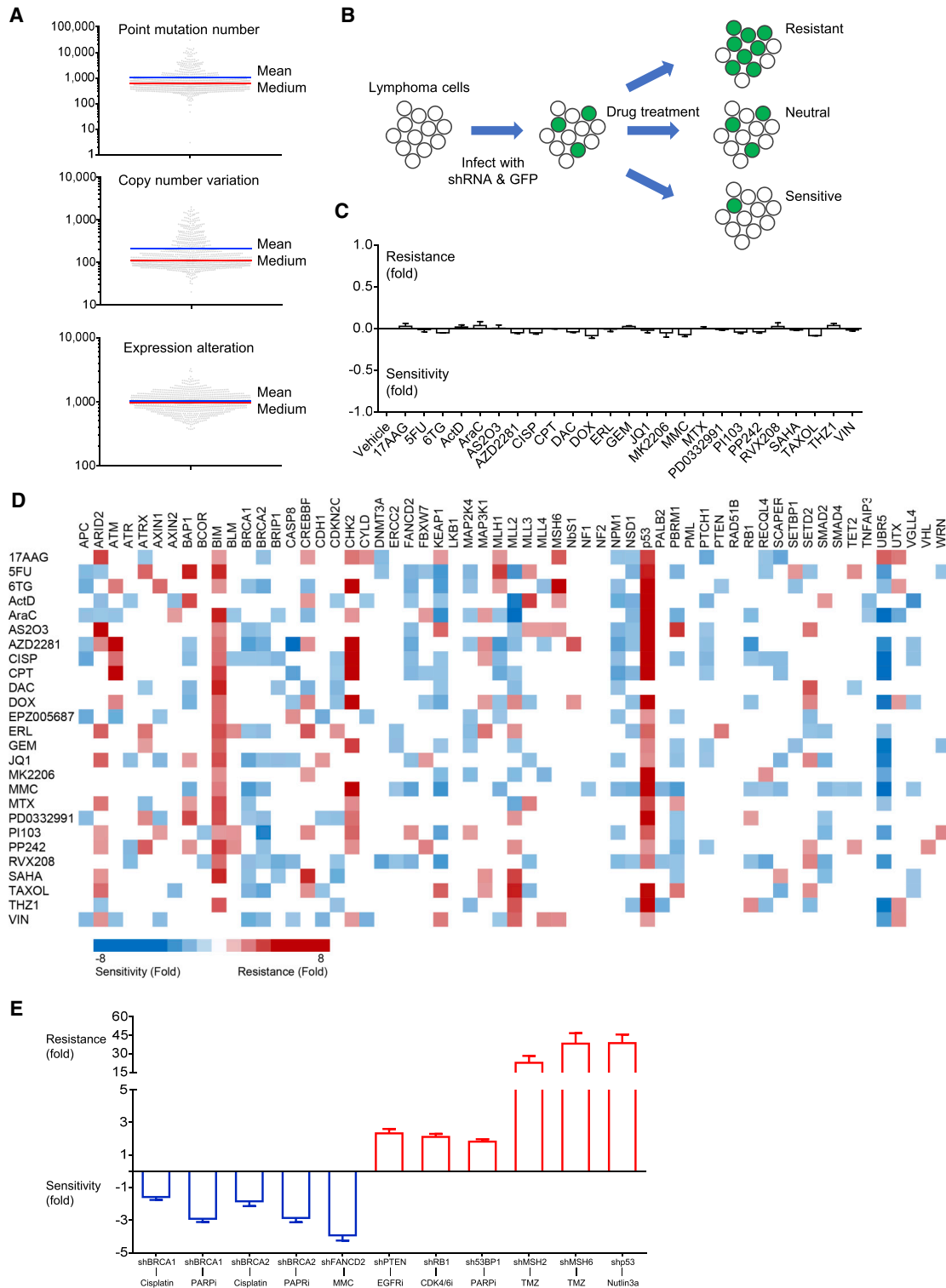


**Figure 1. A Drug Sensitivity Map Describing Changes of Drug Sensitivity upon Depletion of Tumor Suppressor Genes**

(A) Genomic and transcriptional abnormalities in human cancer cell lines. Data were collected from the COSMIC cell line database. A total of 1,019 cell lines were analyzed. Each dot represents data information of a cell line. Shown are the overall distribution of number of point mutations, the number of copy number variations, and the number of over or under-expressed genes from the 1,019 cell lines.

(legend continued on next page)

involved in drug transportation, drug metabolism, maintenance of drug target, bypass survival, and cell death signaling could be among the vastly diverse genetic and transcriptional landscapes among different cell lines. The difference in these genes could have a greater impact on drug sensitivities than the status of tumor suppressor itself. In the presence of such a vast number of variables among cancer cell lines, assuming that drug sensitivity change is caused by the queried gene itself, which is the basis for cell line comparison-based approaches, may result in incorrect predictions.

Moreover, in a recent study, it was shown that cancer cell lines used in labs commonly undergo genetic and transcriptional diversification (Ben-David et al., 2018), which results in the generation of sub-clones that exhibit altered drug sensitivity. This will introduce additional variables that further impair the accuracy of cell line comparison-based approaches.

Because the vast number of variables among cancer cell lines may have compromised the resolution on tumor suppressor-drug interactions, we argue that it is necessary and beneficial to initially explore this question in a more defined, single-variable manner. Given the complex nature of differences between cancer cell lines and their potential impacts on drug sensitivity studies, we first used a single cancer cell line, introduced tumor suppressor deficiency via short hairpin RNA (shRNA)-mediated knockdown, and analyzed whether it altered drug sensitivity. In this manner, changes in drug sensitivities can be attributed to deficiency of the queried tumor suppressor alone, rather than thousands of hard-to-quantify variables between different cancer cell lines. This offers a more defined system that could help identify drug vulnerabilities conferred by tumor suppressor loss. Through this study, we are able to construct a comprehensive map of drug sensitivity changes caused by tumor suppressor loss and to identify many previously unknown tumor suppressor-drug interactions, which may point to new directions for exploiting cancer cells' weaknesses.

## RESULTS

### Systematic Analysis of Drug Sensitivity Conferred by Tumor Suppressor Loss

We previously developed an experimental platform that could detect how a genetic perturbation alters drug sensitivity (Jiang et al., 2011). In several follow up studies, this platform was used to delineate drug mechanism of action (Bruno et al., 2017; Pritchard et al., 2013). In this study, we used this platform to ask how loss of a tumor suppressor may affect drug sensitivity.

Briefly, retrovirus encoding GFP and shRNA against a tumor suppressor was used to partially infect a mouse E $\mu$ -Myc p19<sup>Arf</sup><sup>-/-</sup> lymphoma cell line, which was then treated with an anticancer drug (see STAR Methods for detailed experimental protocols). If depletion of the tumor suppressor sensitized cells to that drug, then in the surviving population, the percentage of GFP-expressing cells will drop (Figure 1B), and the extent of sensitization can be calculated from changes of GFP percentages (Jiang et al., 2011).

Using this approach, the change of drug sensitivity can be attributed to shRNA-mediated tumor suppressor knockdown, because most shRNAs we tested did not affect cell fitness by itself (Data S2), and the retrovirus vector itself did not notably change cellular sensitivities to drugs (Figure 1C).

Several aspects of this platform make it suitable for studying tumor suppressor-drug interactions. First, as an engineered cancer cell line, the E $\mu$ -Myc p19<sup>Arf</sup><sup>-/-</sup> lymphoma cell line has a relatively simple genetic landscape. p53 and major DNA repair pathways remain functional in this cell line, which guards against rapid genetic diversification. We also discard cells when they are in culture for more than 40 days to further reduce the impact of potential genetic and transcriptional diversification on our study. In addition, in our experimental platform (Figure 1B), each sensitivity readout is the collective survival outcome of hundreds of thousands tumor suppressor-deficient and tumor suppressor-proficient cells, and such a large N makes the data highly reproducible (Figure S1A). Moreover, in each experiment, the GFP-negative, tumor suppressor-proficient cells serve as internal controls, significantly reducing the effects of cell passage, cell seeding, serum batch, medium evaporation, and other arcane factors that could have affected the consistencies of MTT-based assays used in cell line comparison-based approaches (Weinstein and Lorenzi, 2013). Using this platform, experiments that were done years apart yielded highly consistent results, and the same gene-drug pairs yielded highly similar resistance or sensitization phenotypes (Figure S1B) (Bruno et al., 2017; Jiang et al., 2011).

Of note, the shRNA vector used in our study is based on the second-generation miR-30-based expression system (Dickins et al., 2005), which helps reduce off-target effects and toxic immune response in host cells (Fellmann et al., 2013; McBride et al., 2008). In order to further limit the impact of off-target effects of shRNA in our study, on average we used three shRNAs for each tumor suppressor gene and tested them separately (see STAR Methods for a detailed discussion). Using this platform, in a one-gene, one-drug manner, we systematically studied how cellular sensitivities to 26 different types of drugs were affected

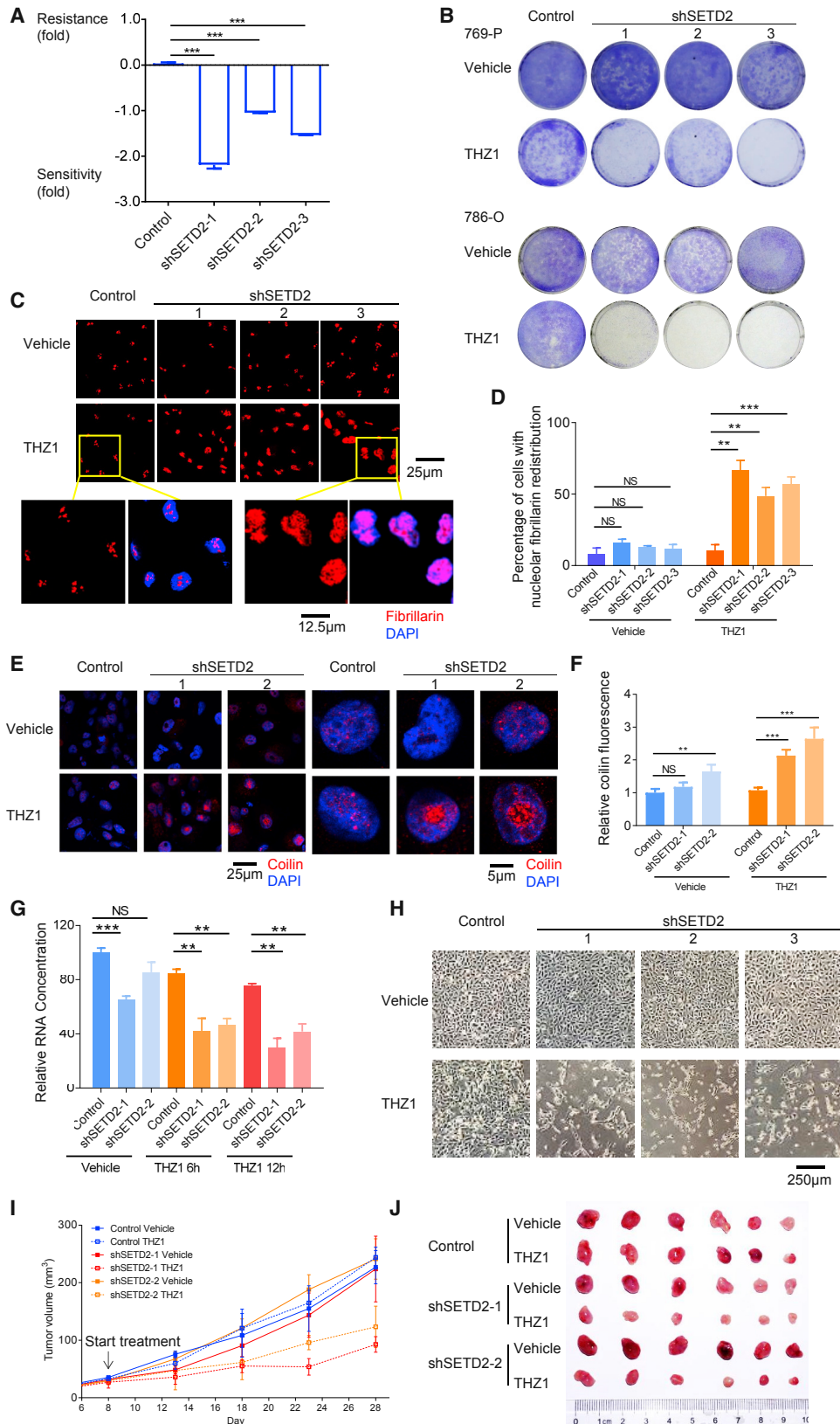
(B) A diagram of GFP-based cell survival competition assay. shRNA and GFP are stably transduced into E $\mu$ -Myc p19<sup>Arf</sup><sup>-/-</sup> lymphoma cells via retroviral infection. If a shRNA alters cellular sensitivity to a certain drug, after drug treatment, the change of sensitivity will manifest as change of GFP-positive cells in surviving cell population. For each experiment, drug-treated samples contain at least 50,000 live cells, and about 1,000 live cells are analyzed using fluorescence-activated cell sorting (FACS).

(C) As control, retrovirus vector alone did not cause significant change in drug sensitivity.

(D) A heatmap summarizing how depletion of tumor suppressor genes causes resistance (red) or sensitivity (blue) to a drug. For each gene, the resistance or sensitivity phenotype is shown if multiple shRNAs exhibit similar resistance or sensitivity phenotype, and average results from these shRNAs are presented in this figure. Data are from at least three independent biological repeats.

(E) Proof-of-principle results showing that depletion of target genes caused expected resistance or sensitivity phenotypes to indicated drugs.

In (C) and (E), data are mean  $\pm$  SEM from at least three independent biological repeats. \*\*\*p < 0.001, \*\*p < 0.01, \*p < 0.05. See also Figure S1 and Tables S1–S5.



(legend on next page)

upon knockdown of 59 genes that frequently exhibit loss of function mutations and/or deletions in human cancers (Figure 1D). The vast majorities of known and potential tumor suppressors in the COSMIC Cancer Gene Census were included in our study. The drugs in this study covered a wide range of anticancer mechanisms, including most types of traditional and targeted therapeutics, as well as recently developed drugs such as BRD4 and CDK7 inhibitors. Strikingly, despite the paucity of current knowledge about tumor suppressor loss-associated drug sensitivities, our results suggested that deficiency of many tumor suppressors could potentially alter sensitivities to various drugs (Figure 1D), thereby providing possible new angles for exploring tumor suppressor-oriented precision cancer medicine.

We first asked whether our approach could faithfully reproduce known associations between tumor suppressor and drug sensitivity. It is known that RB1 deficiency renders cells resistant to CDK4/6 inhibitor (O'Leary et al., 2016), p53 deficiency renders cells resistant to MDM2 inhibitor (Vassilev et al., 2004), BRCA1/2 deficiency causes hypersensitivity to PARP inhibitors and cisplatin (Bryant et al., 2005; Farmer et al., 2005; Tan et al., 2008), MSH2/6 deficiency causes resistance to temozolomide (Friedman et al., 1998), PTEN deficiency renders cells resistant to EGFR inhibitor (Sos et al., 2009), FANCD2 deficiency causes sensitivity to mitomycin C (Unno et al., 2014), and p53BP1 deficiency renders cells resistant to PARP inhibitors (Bunting et al., 2010). As proof of principle (Figure 1E), our method could correctly reproduce 11 of 11 such expected drug sensitivity phenotypes (Table S4). These results accurately reflected clinical observations and the underlying biology. This performance is significantly better than that of the cell line comparison-based approach, which could predict 2 of 11 such gene-drug interactions (Table S3). These proof-of-principle results demonstrated the validity of our method, suggesting that it provides the necessary resolution for delineating tumor suppressor loss-associated drug sensitivities.

Next, from this drug sensitivity map, we chose several novel tumor suppressor-drug interactions, validated them in additional cancer cell lines, and explored the underlying mechanisms.

### SETD2 Deficiency Sensitized Cells to CDK7 Inhibitor

SETD2 is an epigenetic regulator that shows recurrent loss-of-function mutations in kidney cancers (Dalglish et al., 2010).

Recently, loss of SETD2 has also been shown to significantly accelerate the development of lung (Rogers et al., 2017) and colon (Yuan et al., 2017) cancers. Interestingly, using our platform, SETD2 deficiency was found to confer significantly enhanced sensitivity to the CDK7 inhibitor THZ1 (Figures 1D and 2A). Such a synthetic lethal interaction between CDK7 inhibitor and SETD2 deficiency has not been previously reported. Importantly, this phenotype was seen both in E $\mu$ -Myc p19<sup>Arf</sup><sup>-/-</sup> cells, which we used to generate the drug sensitivity map, and in human kidney cancer cell lines (Figure 2B), in which SETD2 loss of function is clinically relevant.

SETD2 is a histone H3K36 methyltransferase, whose function contributes to transcriptional elongation (Kizer et al., 2005). Inhibition of CDK7 impairs earlier steps of transcription, including initiation and pause release (Kwiatkowski et al., 2014). On this basis, we hypothesized that SETD2 deficiency's negative impact on transcriptional elongation may potentially exacerbate the transcriptional stress caused by CDK7 inhibition. Indeed, CDK7 inhibition profoundly altered the distribution of nucleoli proteins fibrillarin and coilin, indicative of severe transcription stress (Boulon et al., 2010; Bruno et al., 2017), in SETD2-knockdown cells but not in control cells (Figures 2C–2F; Figure S2A). CDK7 inhibitor suppressed RNA transcription more severely in SETD2-knockdown cells (Figure 2G), and such cells underwent rapid cell death upon CDK7 inhibition (Figure 2H). When treated *in vivo*, control tumors were barely affected by CDK7 inhibitor, whereas SETD2-deficient tumors were significantly suppressed by CDK7 inhibitor (Figures 2I and 2J; Figure S2B). Such a novel synthetic lethal interaction between CDK7 inhibitor and SETD2 deficiency may inform the clinical development of CDK7 inhibitors, and it also points to new potential opportunity of treating SETD2-deficient cancers in a targeted manner.

### CREBBP Deficiency Confers Resistance to EGFR Inhibitor

CREBBP is a histone acetyltransferase and tumor suppressor recently found to be commonly mutated in lymphoma and leukemia (Mullighan et al., 2011), as well as cancers of the lung (Campbell et al., 2016), bladder (Guo et al., 2013), uterus, and colon. Our drug sensitivity map showed that loss of CREBBP caused significant resistance to EGFR inhibitor (Figures 1D and 3A). Using an EGFR-driven human lung cancer cell line PC-9, we further

#### Figure 2. SETD2 Deficiency Sensitized Cells to CDK7 Inhibitor

(A) Effect of SETD2 depletion on E $\mu$ -Myc p19<sup>Arf</sup><sup>-/-</sup> cells' sensitivity to CDK7 inhibitor THZ1. Data are mean  $\pm$  SEM, from at least three independent biological repeats. \*\*\*p < 0.001, \*\*p < 0.01, \*p < 0.05.

(B) SETD2 depletion sensitized human kidney cancer cell lines to THZ1 treatment. Data are representative results from three independent biological repeats.

(C and D) THZ1 caused significant redistribution of nucleolar protein fibrillarin in SETD2-depleted 769-P cells (C); scale bar as indicated in the figure. Percentage of cells with nucleolar fibrillarin redistribution is shown in (D). Data are mean  $\pm$  SEM from three independent biological repeats. \*\*\*p < 0.001, \*\*p < 0.01, \*p < 0.05.

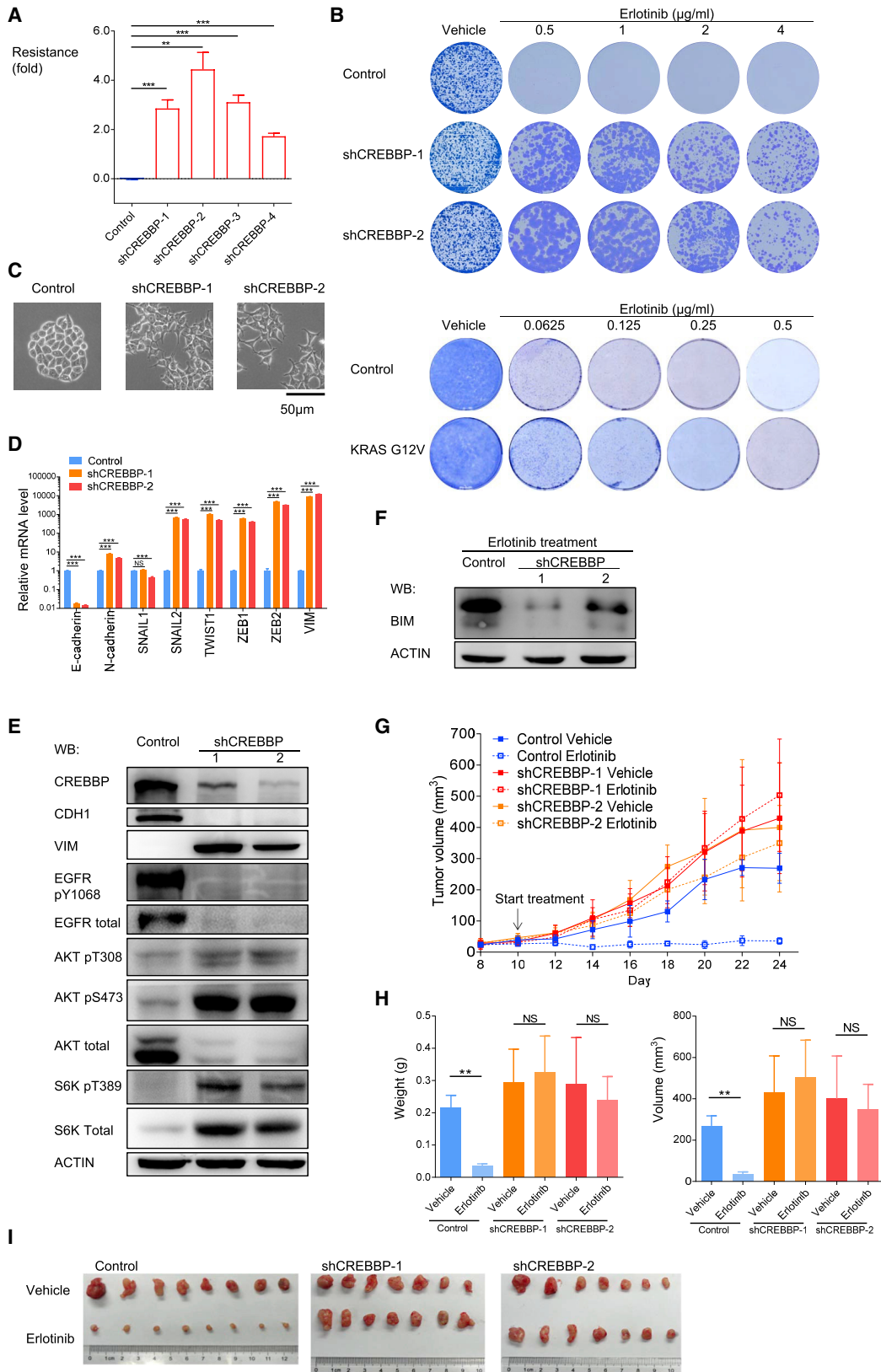
(E and F) THZ1 caused significant redistribution of coilin in SETD2-depleted 769-P cells (E); scale bar as indicated in the figure. Quantitative analysis of results is shown in (F). Data are mean  $\pm$  SEM from three independent biological repeats and passed a Kolmogorov-Smirnov normality test. \*\*\*p < 0.001, \*\*p < 0.01, \*p < 0.05.

(G) RNA expression level in SETD2-depleted 769-P cells was more severely afflicted when treated with THZ1. Data are mean  $\pm$  SEM from three independent biological repeats. \*\*\*p < 0.001, \*\*p < 0.01, \*p < 0.05.

(H) THZ1 treatment caused significant cell death in SETD2-depleted 769-P cells. Scale bar, 250  $\mu$ m.

(I and J) SETD2 depletion enhanced response to THZ1 *in vivo*. Control and SETD2-depleted OS-RC-2 cells were injected into nude mice, and the resulting tumors (n = 6) were treated with vehicle or THZ1 (5 mg/kg once a day). The kidney cancer cell line OS-RC-2 was able to form tumor in nude mice and therefore chosen for this experiment. The tumor volume of each group was assessed every 5 days (I). Data are mean  $\pm$  SD. Images show the dissected tumors 28 days after injection (J). Tumor masses and volumes for each group are shown in Figure S2B.

See also Figure S2.



(legend on next page)

confirmed that loss of CREBBP indeed conferred significant resistance to the EGFR inhibitor erlotinib, even at very high dose (Figure 3B). In contrast, the expression of KRAS G12V mutant also protected PC-9 cells from erlotinib, but only at much lower drug doses (Figure 3B). This suggests that CREBBP status may significantly modulate the treatment efficacy of EGFR inhibitor.

For targeted therapeutics such as EGFR inhibitors, there are several routes leading to their clinical resistance, including EGFR mutation such as T790M (Kobayashi et al., 2005; Pao et al., 2005), mutations of downstream genes such as KRAS, and upregulation of other kinases such as c-MET (Engelman et al., 2007). Beside these, another clinically observed cause of resistance is cell state conversion (Shaffer et al., 2017; Viswanathan et al., 2017), in which cancer cells transit from epithelial to mesenchymal state and become resistant to EGFR inhibitors (Byers et al., 2013; Thomson et al., 2005; Yauch et al., 2005). However, the mechanism behind such observation remains elusive. Interestingly, upon knockdown of CREBBP, PC-9 cells displayed striking features of epithelial-to-mesenchymal transition (EMT), including spindle-shaped morphology (Figure 3C), as well as drastic transcriptional changes consistent with EMT (Figures 3D and 3E). Interestingly, upon EMT, CREBBP-deficient cells lost the expression of EGFR (Figure 3E) but still maintained viability. When treated with EGFR inhibitors, such cells did not respond properly and failed to effectively upregulate BIM, a pro-apoptotic gene essential for EGFR-induced cell death and its clinical efficacy (Ng et al., 2012) (Figure 3F). When treated *in vivo*, control PC-9 tumors were nearly completely suppressed by EGFR inhibitor, whereas the growth of CREBBP-deficient PC-9 tumors was largely unaffected by EGFR inhibitor (Figures 3G–3I). This suggested that CREBBP status may significantly modulate the outcome of treatment by EGFR inhibitors. Currently, a tractable model of EMT-induced targeted therapeutic resistance is still being sought for, and our results showed that loss of the tumor suppressor CREBBP could provide an epigenetic switch that leads to both EMT and drug resistance.

Of note, CREBBP knockdown does not affect cell growth in tissue culture (Figure 3B). In the *in vivo* experiment, it appears that CREBBP-knockdown tumors have a trend to grow faster than control group tumors (Figure 3G). It is possible that CREBBP knockdown may help cells adapt to *in vivo* challenges, such as nutrients, metabolic changes, hypoxia, and so on. However, the near absence of response to EGFR inhibitor (Figure 3I)

in CREBBP-knockdown groups still demonstrates that CREBBP deficiency causes resistance to EGFR inhibitor *in vivo*.

### CREBBP Depletion Sensitized Cells to DNA-Damage Drugs

Given CREBBP's important roles in many cellular processes, we further asked whether CREBBP loss may cause associated weakness for certain types of anticancer drugs.

In E $\mu$ -Myc p19<sup>Arf</sup><sup>-/-</sup> cells, we observed that loss of CREBBP significantly sensitized cells to treatment by several drugs, including cisplatin, 6-TG, and camptothecin (Figures 1D and 4A). Through various means, these drugs cause cellular DNA damage. Cells cope with such stress by eliciting an ATR-CHK1 response to establish early S-phase arrest, in order to stop further damage and to provide time for DNA repair. A previous study indicated that CREBBP participates in the ATR-CHK1 signaling cascade (Stauffer et al., 2007), and our results suggest that this may cause a synthetic lethal interaction between CREBBP deficiency and DNA-damage drugs. Indeed, in lung cancer cell line PC-9 and bladder cancer cell line UM-UC-3, control cells were arrested in early S phase when treated with camptothecin, whereas in CREBBP-deficient cells, DNA replication proceeded to late S or G2/M stage (Figure 4B). As a result, more DNA damage accumulated in CREBBP-deficient cells, as evidenced by increased H2AX phosphorylation upon camptothecin treatment (Figure 4C). Long-term colony formation assays also confirmed that CREBBP loss significantly reduced cell survival upon camptothecin treatment (Figure 4D). When treated *in vivo*, tumors form by CREBBP-knockdown PC-9 cells shrank more dramatically in response to irinotecan (Figures 4E and 4F), which is a camptothecin-derivative drug used in clinics. This suggests the CREBBP-DNA-damage drug interaction may significantly alter treatment outcome.

We further asked whether existing clinical data support this observation. In human patients, lung squamous cancers are mostly treated with chemotherapeutic drugs that attack DNA. Survival analysis of The Cancer Genome Atlas (TCGA) lung squamous cancer database using SurvExpress (Aguirre-Gamboa et al., 2013) suggested that the survival rate of CREBBP-low cancer patients is significantly better than that of CREBBP-high cancer patients (Figure 4G). This is consistent with our finding that CREBBP deficiency sensitizes cancer cells to DNA-damage drugs. It further shows that traditional anticancer drugs, when applied to target the weakness caused by certain tumor

### Figure 3. CREBBP Depletion Conferred Resistance to EGFR Inhibitors

(A) Effect of CREBBP depletion on E $\mu$ -Myc p19<sup>Arf</sup><sup>-/-</sup> cells' sensitivity to EGFR inhibitor erlotinib. Data are mean  $\pm$  SEM from at least three independent biological repeats. \*\*\*p < 0.001, \*\*p < 0.01, \*p < 0.05.

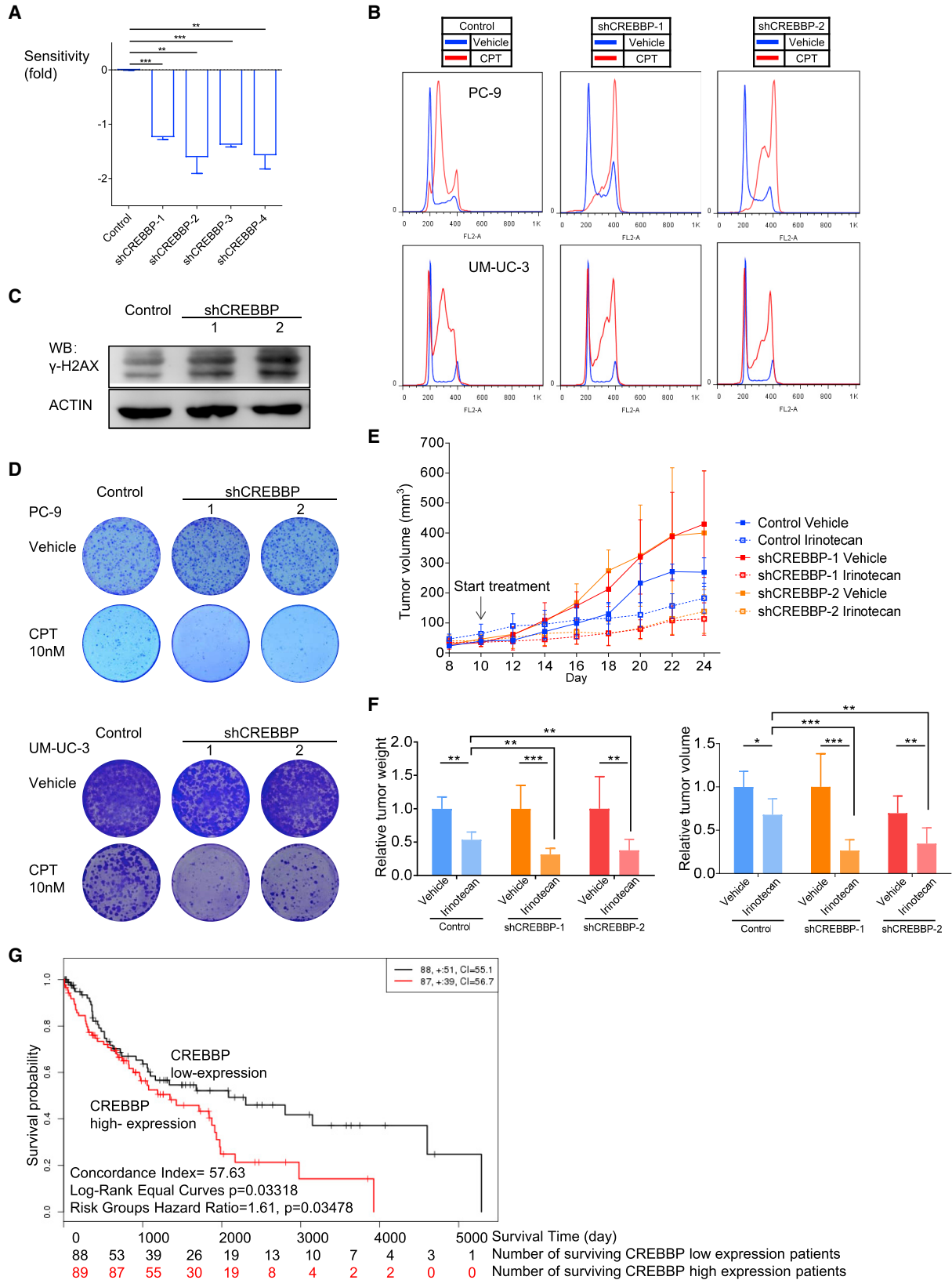
(B) CREBBP depletion caused resistance to EGFR inhibition. The upper and lower panels show how CREBBP knockdown and expression of KRAS mutant affected PC-9 cells' sensitivity to erlotinib. Data are representative results from three independent biological repeats.

(C) CREBBP depletion caused EMT in PC-9 cells. Scale bar, 50  $\mu$ m.

(D and E) RNA (D) and protein (E) levels of EMT markers and EGFR and AKT signaling in PC-9 cells after CREBBP depletion. Data are mean  $\pm$  SEM from three independent biological repeats in (D). \*\*\*p < 0.001, \*\*p < 0.01, \*p < 0.05.

(F) CREBBP-depleted PC-9 cells failed to efficiently upregulate BIM after erlotinib treatment. Control and CREBBP-knockdown PC-9 cells were treated with 0.2  $\mu$ g/mL erlotinib for 24 h and analyzed using western blot.

(G–I) CREBBP depletion abolished response to erlotinib *in vivo*. Control and CREBBP-depleted PC-9 cells were injected into nude mice, and the resulting tumors (n = 7) were treated with vehicle or erlotinib (16 mg/kg once a day). The tumor volume of each group was assessed every 2 days (G). Tumor masses and volumes for each group are shown in (H). Data are mean  $\pm$  SD. Images show the dissected tumors 24 days after injection (I). \*\*\*p < 0.001, \*\*p < 0.01, \*p < 0.05.



(legend on next page)

suppressor loss, can also potentially lead to better treatment outcome.

### BAP1 Deficiency Sensitized Cells to Inhibitors of DNMT1 and PARP

BAP1 is a newly discovered tumor suppressor significantly mutated in clear cell renal carcinoma (Peña-Llopis et al., 2012), uveal melanoma (Harbour et al., 2010), and mesothelioma (Testa et al., 2011). Our results showed that multiple shRNAs targeting BAP1 led to enhanced sensitivities toward DNMT1 inhibitor (Figures 1D and 5A). This prompted us to examine the potential relationship between BAP1 and DNMT1.

Interestingly, upon BAP1 knockdown, the protein level of DNMT1 significantly decreased (Figure 5B; Figure S3A), which may explain why BAP1-deficient cells are more sensitive to DNMT1 inhibitors. BAP1 knockdown did not change the mRNA level of DNMT1 (Figure 5C; Figure S3B), which prompted us to ask whether BAP1 modulates DNMT1 at the post-translational level.

Given that BAP1 is a deubiquitinase, we asked whether BAP1 controlled DNMT1 protein stability. Indeed, treatment of BAP1-deficient cells with proteasome inhibitor restored DNMT1 protein level (Figure 5D). Next, using co-immunoprecipitation assays, we found that BAP1 and DNMT1 interact with each other (Figure 5E; Figure S3C). Furthermore, the expression of full-length BAP1, but not a mutant that lacks deubiquitinase activity, reduced the ubiquitination level of DNMT1 (Figure 5F). Expression of BAP1 also significantly prolonged the half-life of endogenous DNMT1 from 8 to more than 24 h (Figures 5G and 5H).

Taken together, these data suggest that BAP1 may act as a novel deubiquitinase for DNMT1, and it controls DNMT1 protein stability. Consequently, cells with BAP1 deficiency have lower levels of DNMT1 (Figure 5B; Figure S3A) and are more sensitive to DNMT1 inhibitor decitabine, which we further confirmed using a human kidney cancer cell line (Figure 5I). These findings show that BAP1 deficiency may cause hypersensitivity to DNMT1 inhibitors, which may provide new angles of targeting BAP1-deficient cancers.

## DISCUSSION

Deficiency of tumor suppressors may bring associated weakness that could potentially be used in cancer therapy. The syn-

thetic lethal interactions between BRCA1/2 deficiency and PARP inhibitors (Bryant et al., 2005; Farmer et al., 2005) has led to improved treatment strategies for ovarian (Kaufman et al., 2015; Ledermann et al., 2016) and breast cancers (Robson et al., 2017; Tutt et al., 2010).

However, unlike oncogenes, tumor suppressor loss does not offer direct ways to exploit in cancer treatment. Therefore, despite the prevalence of tumor suppressor mutations in cancer genomes, the full spectrum of drug sensitivity conferred by tumor suppressor loss remains unknown, which greatly hampers the utility of tumor suppressor loss in precision cancer medicine.

The presence of aberrantly activated oncogene often dictates an all-or-none response to its targeted drugs. However, for tumor suppressor, such a strong and intuitive gene-drug interaction is not expected. The highly diverse genetic and transcriptional landscapes of different cancer cell lines may have rendered it difficult to study tumor suppressor-drug interactions, given that the presence of too many other variables, rather than the tumor suppressor itself, may significantly modulate drug response. As a result, the cell line comparison-based approaches led to a rather limited number of novel tumor suppressor-drug interactions (Table S1) and failed to recapitulate most known tumor suppressor-drug interactions (Table S3).

In light of this, we analyzed how tumor suppressor deficiency may modulate drug sensitivity in a more defined, single-variable manner. First, with regard to existing tumor suppressor-drug interaction knowledge, our approach performed significantly better (Figure 1E). In our study of 59 common tumor suppressors in the COSMIC Cancer Gene Census and 26 different types of anticancer drugs, we uncovered many previously unknown gene-drug interactions (Figure 1D) that may help shed light on how to exploit tumor suppressor deficiency in precision cancer medicine. We also observed that the gene-drug interaction signatures could help group drugs with similar mechanism of action (Figure 6A). For example, DNA-damage drugs, microtubule poisons, and bromodomain inhibitors each registered specific gene-drug resistance-sensitivity patterns that help group these drugs. This provides additional evidence that our drug sensitivity results reflect underlying biological mechanisms. We further studied drug sensitivities associated with SETD2, CREBBP, and BAP1 deficiency and identified the underlying mechanisms, which may provide new angles of attacking cancers with such deficiencies.

### Figure 4. CREBBP Depletion Sensitized Cells to Topoisomerase I Inhibitor

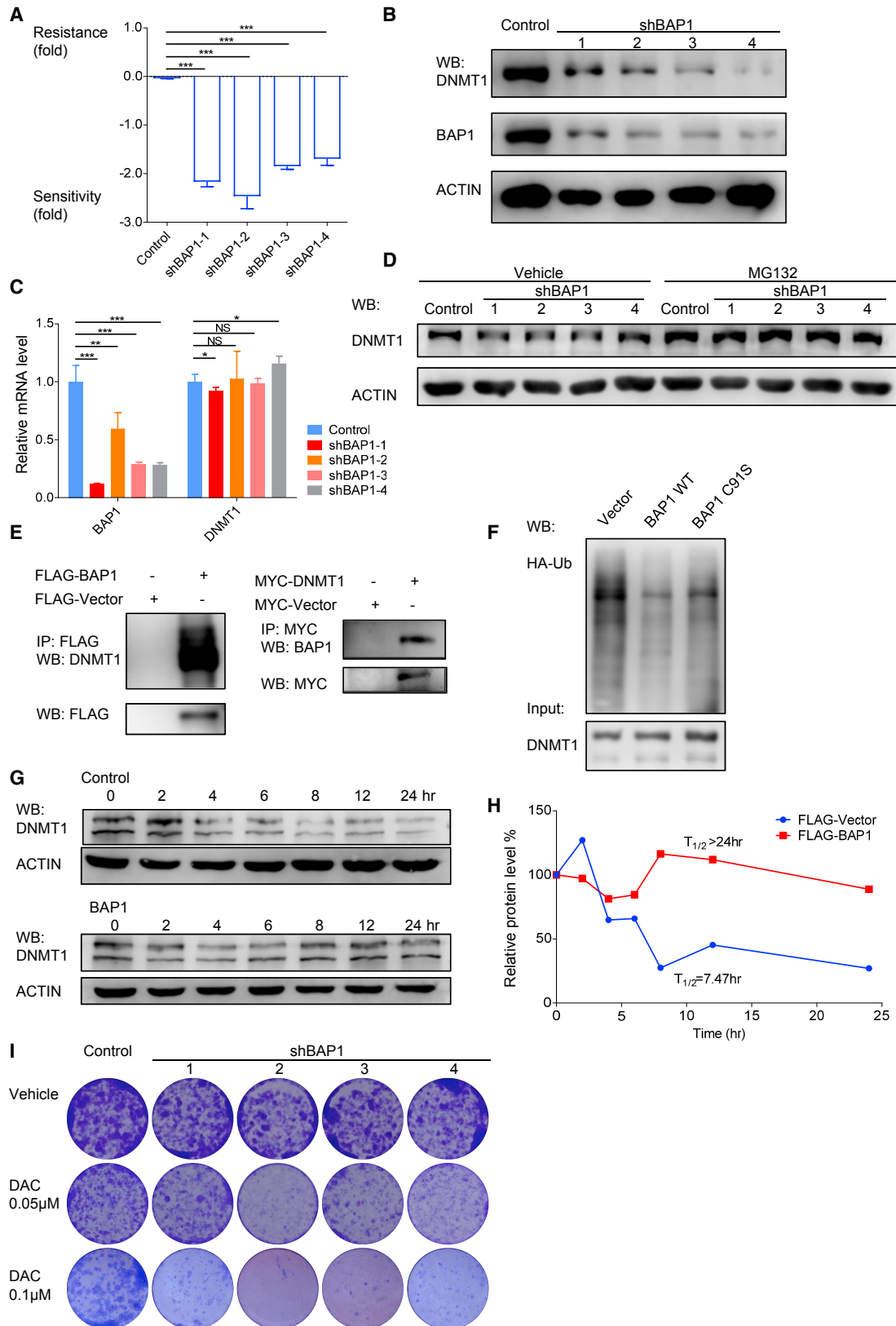
(A) Effect of CREBBP depletion on E $\mu$ -Myc p19<sup>Arf</sup><sup>-/-</sup> cells' sensitivity to topoisomerase I inhibitor camptothecin. Data are mean  $\pm$  SEM from at least three independent biological repeats. \*\*\*p < 0.001, \*\*p < 0.01, \*p < 0.05.

(B) In human lung cancer cell line PC-9 and human bladder cancer cell line UM-UC-3, CREBBP depletion impaired cell cycle checkpoint after camptothecin (CPT) treatment.

(C) CREBBP-depleted cells accumulated more DNA damage after camptothecin treatment.

(D) CREBBP depletion sensitized two human cancer cells to camptothecin. Data are representative results from three independent biological repeats.

(E and F) CREBBP depleted cells were sensitive to irinotecan, which is a water-soluble derivative of camptothecin *in vivo*. Control and CREBBP-depleted PC-9 cells were injected into nude mice, and the resulting tumors were treated with vehicle or irinotecan (50 mg/kg intraperitoneally every 4 days). Tumor sizes (n = 7) were monitored every 2 days (E). Data are mean  $\pm$  SD. This experiment was executed together with that depicted in Figure 3G and shared the same vehicle group. Relative tumor weight and volume were calculated of the dissected tumors 24 days after injection (F). Data are mean  $\pm$  SD. \*\*\*p < 0.001, \*\*p < 0.01, \*p < 0.05. (G) The correlation of survival with CREBBP gene expression in patients with lung squamous cancer. Kaplan-Meier survival curves were constructed using the SurvExpress program for the analysis of samples of TCGA LUSC datasets. Red and black curves denote high- and low-risk groups respectively. The y axis indicates the percentage of survival. The x axis represents survival days, and the bottom two rows of numbers indicate the number of survivors in CREBBP low expression (in black) and high expression (in red) at the corresponding time.



(legend on next page)

In this study we aimed to provide additional hypothesis for exploring potential weakness associated with tumor suppressor loss. However, gene-drug interactions can be cell type dependent, and some of the phenotypes we discovered in E $\mu$ -Myc p19<sup>Arf-/-</sup> cells (Figure 1D) may not translate in other cell types. With this in mind, we used an additional BCR-ABL driven ALL cell line (Williams et al., 2006) to test those strong resistance and sensitization phenotypes we observed in E $\mu$ -Myc p19<sup>Arf-/-</sup> cells (Figure 1D). Overall, resistance and sensitization phenotypes are highly consistent in both cell lines (Figure 6B; Table S5). This suggests that the strong resistance and sensitization phenotypes we report here point to certain gene-drug interactions that are crucial for determining drug sensitivity. However, such gene-drug interactions may still be cell context dependent. If in some lineage of cells, gene expression landscape renders some repair pathway ineffective, certain gene-drug interactions may not apply. For example, in a recent publication (Herbert et al., 2019), a tissue-restricted transcription factor, BRN2, was shown to interact with multiple proteins that are important for DNA damage repair. In addition to reprogramming DNA repair pathway, BRN2 also suppresses the expression of pro-apoptotic genes. Therefore, certain gene-drug interactions may be blunted or blocked in cancer types that express BRN2. On the other hand, it is also possible that in some lineages of cancers, gene expression landscape will enable certain gene-drug interactions that are not discovered in E $\mu$ -Myc p19<sup>Arf-/-</sup> cells.

Given that tumor suppressors are frequently disabled in cancers, they may present natural stratifies for precision therapy in significant portions of patients. Our study yielded a systematic view of potential tumor suppressor-drug interaction and suggested that deficiency in many tumor suppressors could strongly alter cellular sensitivity to certain drugs. This may provide a much needed starting point for forming hypothesis about how to use tumor suppressor loss in cancer therapy. Such approaches can be applied either as single therapy targeting tumor suppressor deficiency itself or in conjunction with other types of therapies. For example, recently anticancer drugs have been used together with immune therapy, with the goal of releasing cancer neo-antigens through drug-induced cell death, thereby facilitating immune clearance of tumors. Knowing the drug vulnerabilities conferred by tumor suppressor loss could potentially help inform the design of such combination immune therapies.

In addition, we observed that in some cases, loss of a tumor suppressor could sensitize cancer cells to multiple types of

drugs, which may provide the basis for combinatorial precision treatment. For example, BAP1 deficiency sensitized cancer cells to DNMT1 inhibitor (Figure 5). We also observed that loss of BAP1 caused significant sensitivity to PARP inhibitor (Figure S3D), which is consistent with BAP1's role in homologous recombination (Yu et al., 2014). Given that BAP1 loss sensitized cells to both PARP inhibitor and DNMT1 inhibitor, two drugs with vastly different anticancer mechanisms, we asked whether combined treatment of BAP1-deficient cancer cells with these two drugs could achieve further enhanced efficacy. Indeed, combining PARP inhibitor and DNMT1 inhibitor, each at reduced dose, produced more significant killing of BAP1-deficient cells than either drug alone (Figure S3E). This highlights the possibility of attacking weaknesses associated with tumor suppressor loss with multiple drugs, which may help maximally eliminate cancer cells.

Last, many tumor suppressors were recently discovered from cancer genome sequencing studies, and our understanding of their biological functions remains incomplete. Given that the drugs used in our study contain a wide range of perturbants of important cellular pathways and processes, this chemical-genetic interaction map also sheds light on the biological functions of tumor suppressors. For example, the observation of BAP1-deficient cells' sensitivity to DNMT1 inhibitor led to the discovery that BAP1 regulates DNMT1 protein stability. Therefore, this systematic chemical-genetic interaction map could also provide valuable clues to the biological functions of newly discovered tumor suppressors.

## STAR★METHODS

Detailed methods are provided in the online version of this paper and include the following:

- KEY RESOURCES TABLE
- CONTACT FOR REAGENT AND RESOURCE SHARING
- EXPERIMENTAL MODEL AND SUBJECT DETAILS
  - Cell lines
  - Mice
- METHOD DETAILS
  - GFP-based cell survival competition assay to determine sensitivity change caused by tumor suppressor loss
  - Calculation of relative resistance/sensitivity from GFP-based cell survival competition assay

### Figure 5. BAP1 Depletion Sensitized Cells to DNMT1 Inhibitor

(A) Effect of BAP1 depletion on E $\mu$ -Myc p19<sup>Arf-/-</sup> cells' sensitivity to DNMT1 inhibitor decitabine (DAC). Data are mean  $\pm$  SEM from at least three independent biological repeats. \*\*\*p < 0.001, \*\*p < 0.01, \*p < 0.05.

(B) BAP1 depletion led to reduced DNMT1 protein level in human kidney cancer 786-O cells.

(C) qPCR analysis of knockdown efficiency of BAP1 and its effect on DNMT1 RNA level in human kidney cancer 786-O cells. Data are mean  $\pm$  SEM from three independent biological repeats. \*\*\*p < 0.001, \*\*p < 0.01, \*p < 0.05.

(D) Proteasome inhibition restored DNMT1 protein level in BAP1-depleted cells.

(E) Co-immunoprecipitation assay showing interaction between ectopic BAP1 and endogenous DNMT1 and interaction between ectopic DNMT1 and endogenous BAP1.

(F) Expression of wild-type (WT) BAP1, but not a deubiquitinase-defective C91S mutant reduced DNMT1 ubiquitination level.

(G and H) Expression of BAP1 extended half-life of DNMT1 in HEK293T cells. Protein level of DNMT1 was measured by western blot (G) and was used to generate half-life curve of DNMT1 (H).

(I) BAP1 depletion sensitized 786-O cells to decitabine. Data are representative results from three independent biological repeats.

See also Figure S3.

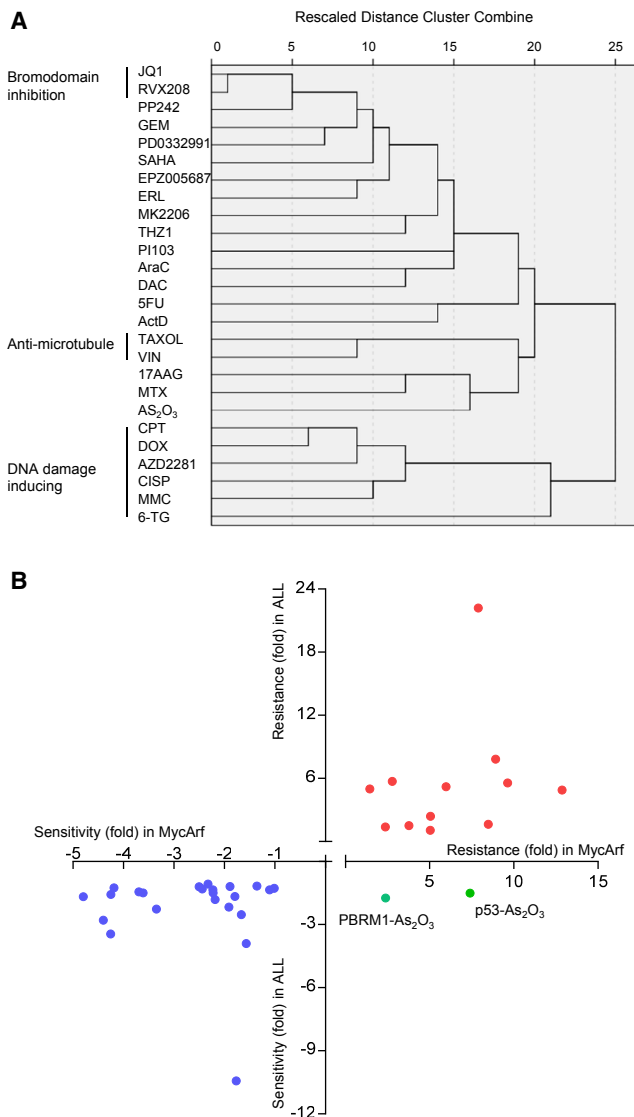


**Figure 6. Additional Analysis of Gene-Drug Interactions Generated in E $\mu$ -Myc p19<sup>Arf</sup><sup>-/-</sup> Cells**

(A) Unsupervised hierarchical clustering of different drugs according to their resistance or sensitization “signatures” registered with 59 tumor suppressors. Hierarchical clustering was performed in SPSS 20.0 software. All gene-drug interactions were calculated for cluster on the basis of drug. The cluster method is between-groups linkage, and the interval measure is squared Euclidean distance.

(B) Comparison of gene-drug interactions in E $\mu$ -Myc p19<sup>Arf</sup><sup>-/-</sup> cells and BCR-ABL ALL cells. Each dot represents a gene-drug pair. The x axis represents the level of resistance or sensitization in E $\mu$ -Myc p19<sup>Arf</sup><sup>-/-</sup> cells, and the y axis represents the level of resistance or sensitization in BCR-ABL ALL cells. Each dot represents the average of resistance or sensitization scores of at least three independent biological repeats.

- Cell line comparison-based data acquisition
- Constructs
- Cell cycle analyses
- Western Blot and Immunoprecipitation
- Immunofluorescence staining

- Colony formation assay
- RNA extraction and qRT-PCR
- Ubiquitination assay
- Generation of nude mice xenografts and drug treatment
- Kaplan-Meier survival curve
- **QUANTIFICATION AND STATISTICAL ANALYSIS**
- **DATA AND SOFTWARE AVAILABILITY**

#### SUPPLEMENTAL INFORMATION

Supplemental Information can be found online at <https://doi.org/10.1016/j.celrep.2019.05.043>.

#### ACKNOWLEDGMENTS

This work was supported by the major scientific research project from the Ministry of Science and Technology of China (grant 2017YFA0504503, 2013CB910404), Strategic Priority Research Program of the Chinese Academy of Sciences (grant XDB19000000), and the National Natural Science Foundation of China (grant 31371418, 81572756). We thank Dr. Dangsheng Li for discussions and helpful comments and the Animal Core Facility and Core Facility for Cell Biology at the Shanghai Institute of Biochemistry and Cell Biology (SIBCB).

#### AUTHOR CONTRIBUTIONS

H.J. conceived the study and wrote the manuscript. H.D., J.Z., Y.Z., J.Y., M.L., L.X., X.L., M.L., and C.L. cloned shRNA constructs and collected drug sensitivity data. H.D. and J.Z. performed other experiments with participation from Z.H. and S.C. Data analysis and interpretation were performed by H.D. and J.Z. All authors discussed the results and commented on the manuscript. H.J. supervised the study.

#### DECLARATION OF INTERESTS

These authors declare no competing interests.

Received: September 16, 2018

Revised: March 21, 2019

Accepted: May 10, 2019

Published: June 11, 2019

#### REFERENCES

- Aguirre-Gamboa, R., Gomez-Rueda, H., Martínez-Ledesma, E., Martínez-Torrey, A., Chacolla-Huaranga, R., Rodríguez-Barrientos, A., Tamez-Peña, J.G., and Treviño, V. (2013). SurvExpress: an online biomarker validation tool and database for cancer gene expression data using survival analysis. *PLoS ONE* 8, e74250.
- Barretina, J., Caponigro, G., Stransky, N., Venkatesan, K., Margolin, A.A., Kim, S., Wilson, C.J., Lehár, J., Kryukov, G.V., Sonkin, D., et al. (2012). The Cancer Cell Line Encyclopedia enables predictive modelling of anticancer drug sensitivity. *Nature* 483, 603–607.
- Ben-David, U., Siranosian, B., Ha, G., Tang, H., Oren, Y., Hinohara, K., Strathdee, C.A., Dempster, J., Lyons, N.J., Burns, R., et al. (2018). Genetic and transcriptional evolution alters cancer cell line drug response. *Nature* 560, 325–330.
- Boulon, S., Westman, B.J., Hutten, S., Boisvert, F.M., and Lamond, A.I. (2010). The nucleolus under stress. *Mol. Cell* 40, 216–227.
- Bric, A., Miething, C., Bialucha, C.U., Scuoppo, C., Zender, L., Krasnitz, A., Xuan, Z., Zuber, J., Wigler, M., Hicks, J., et al. (2009). Functional identification of tumor-suppressor genes through an in vivo RNA interference screen in a mouse lymphoma model. *Cancer Cell* 16, 324–335.

- Bruno, P.M., Liu, Y., Park, G.Y., Murai, J., Koch, C.E., Eisen, T.J., Pritchard, J.R., Pommier, Y., Lippard, S.J., and Hemann, M.T. (2017). A subset of platinum-containing chemotherapeutic agents kills cells by inducing ribosome biogenesis stress. *Nat. Med.* **23**, 461–471.
- Bryant, H.E., Schultz, N., Thomas, H.D., Parker, K.M., Flower, D., Lopez, E., Kyle, S., Meuth, M., Curtin, N.J., and Helleday, T. (2005). Specific killing of BRCA2-deficient tumours with inhibitors of poly(ADP-ribose) polymerase. *Nature* **434**, 913–917.
- Bunting, S.F., Callén, E., Wong, N., Chen, H.-T., Polato, F., Gunn, A., Bothmer, A., Feldhahn, N., Fernandez-Capetillo, O., Cao, L., et al. (2010). 53BP1 inhibits homologous recombination in Brca1-deficient cells by blocking resection of DNA breaks. *Cell* **141**, 243–254.
- Burgess, D.J., Doles, J., Zender, L., Xue, W., Ma, B., McCombie, W.R., Hannon, G.J., Lowe, S.W., and Hemann, M.T. (2008). Topoisomerase levels determine chemotherapy response in vitro and in vivo. *Proc. Natl. Acad. Sci. U S A* **105**, 9053–9058.
- Byers, L.A., Diao, L., Wang, J., Saintigny, P., Girard, L., Peyton, M., Shen, L., Fan, Y., Giri, U., Tumula, P.K., et al. (2013). An epithelial-mesenchymal transition gene signature predicts resistance to EGFR and PI3K inhibitors and identifies Axl as a therapeutic target for overcoming EGFR inhibitor resistance. *Clin. Cancer Res.* **19**, 279–290.
- Campbell, J.D., Alexandrov, A., Kim, J., Wala, J., Berger, A.H., Pedamallu, C.S., Shukla, S.A., Guo, G., Brooks, A.N., Murray, B.A., et al.; Cancer Genome Atlas Research Network (2016). Distinct patterns of somatic genome alterations in lung adenocarcinomas and squamous cell carcinomas. *Nat. Genet.* **48**, 607–616.
- Dalgliesh, G.L., Furge, K., Greenman, C., Chen, L., Bignell, G., Butler, A., Davies, H., Edkins, S., Hardy, C., Latimer, C., et al. (2010). Systematic sequencing of renal carcinoma reveals inactivation of histone modifying genes. *Nature* **463**, 360–363.
- Dickins, R.A., Hemann, M.T., Zilfou, J.T., Simpson, D.R., Ibarra, I., Hannon, G.J., and Lowe, S.W. (2005). Probing tumor phenotypes using stable and regulated synthetic microRNA precursors. *Nat. Genet.* **37**, 1289–1295.
- Engelman, J.A., Zejnullahu, K., Mitsudomi, T., Song, Y., Hyland, C., Park, J.O., Lindeman, N., Gale, C.-M., Zhao, X., Christensen, J., et al. (2007). MET amplification leads to gefitinib resistance in lung cancer by activating ERBB3 signaling. *Science* **316**, 1039–1043.
- Farmer, H., McCabe, N., Lord, C.J., Tutt, A.N.J., Johnson, D.A., Richardson, T.B., Santarosa, M., Dillon, K.J., Hickson, I., Knights, C., et al. (2005). Targeting the DNA repair defect in BRCA mutant cells as a therapeutic strategy. *Nature* **434**, 917–921.
- Fellmann, C., Hoffmann, T., Sridhar, V., Hopfgartner, B., Muhar, M., Roth, M., Lai, D.Y., Barbosa, I.A.M., Kwon, J.S., Guan, Y., et al. (2013). An optimized microRNA backbone for effective single-copy RNAi. *Cell Rep.* **5**, 1704–1713.
- Forbes, S.A., Beare, D., Gunasekaran, P., Leung, K., Bindal, N., Boutselakis, H., Ding, M., Bamford, S., Cole, C., Ward, S., et al. (2015). COSMIC: exploring the world's knowledge of somatic mutations in human cancer. *Nucleic Acids Res.* **43**, D805–D811.
- Friedman, H.S., McLendon, R.E., Kerby, T., Dugan, M., Bigner, S.H., Henry, A.J., Ashley, D.M., Krischer, J., Lovell, S., Rasheed, K., et al. (1998). DNA mismatch repair and O6-alkylguanine-DNA alkyltransferase analysis and response to Temodal in newly diagnosed malignant glioma. *J. Clin. Oncol.* **16**, 3851–3857.
- Futreal, P.A., Coin, L., Marshall, M., Down, T., Hubbard, T., Wooster, R., Rahman, N., and Stratton, M.R. (2004). A census of human cancer genes. *Nat. Rev. Cancer* **4**, 177–183.
- Garnett, M.J., Edelman, E.J., Heidorn, S.J., Greenman, C.D., Dastur, A., Lau, K.W., Greninger, P., Thompson, I.R., Luo, X., Soares, J., et al. (2012). Systematic identification of genomic markers of drug sensitivity in cancer cells. *Nature* **483**, 570–575.
- Guo, G., Sun, X., Chen, C., Wu, S., Huang, P., Li, Z., Dean, M., Huang, Y., Jia, W., Zhou, Q., et al. (2013). Whole-genome and whole-exome sequencing of bladder cancer identifies frequent alterations in genes involved in sister chromatid cohesion and segregation. *Nat. Genet.* **45**, 1459–1463.
- Haibe-Kains, B., El-Hachem, N., Birkbak, N.J., Jin, A.C., Beck, A.H., Aerts, H.J.W.L., and Quackenbush, J. (2013). Inconsistency in large pharmacogenomic studies. *Nature* **504**, 389–393.
- Harbour, J.W., Onken, M.D., Roberson, E.D.O., Duan, S., Cao, L., Worley, L.A., Council, M.L., Matattal, K.A., Helms, C., and Bowcock, A.M. (2010). Frequent mutation of BAP1 in metastasizing uveal melanomas. *Science* **330**, 1410–1413.
- Herbert, K., Binet, R., Lambert, J.-P., Louphrasitthiphol, P., Kalkavan, H., Sesma-Sanz, L., Robles-Espinoza, C.D., Sarkar, S., Suer, E., Andrews, S., et al. (2019). BRN2 suppresses apoptosis, reprograms DNA damage repair, and is associated with a high somatic mutation burden in melanoma. *Genes Dev.* **33**, 310–332.
- Hunter, D.J. (2016). Uncertainty in the Era of Precision Medicine. *N. Engl. J. Med.* **375**, 711–713.
- Iorio, F., Knijnenburg, T.A., Vis, D.J., Bignell, G.R., Menden, M.P., Schubert, M., Aben, N., Goncalves, E., Barthorpe, S., Lightfoot, H., et al. (2016). A landscape of pharmacogenomic interactions in cancer. *Cell* **166**, 740–754.
- Jiang, H., Pritchard, J.R., Williams, R.T., Lauffenburger, D.A., and Hemann, M.T. (2011). A mammalian functional-genetic approach to characterizing cancer therapeutics. *Nat. Chem. Biol.* **7**, 92–100.
- Kaufman, B., Shapira-Frommer, R., Schmutzler, R.K., Audeh, M.W., Friedlander, M., Balmaña, J., Mitchell, G., Fried, G., Stemmer, S.M., Hubert, A., et al. (2015). Olaparib monotherapy in patients with advanced cancer and a germline BRCA1/2 mutation. *J. Clin. Oncol.* **33**, 244–250.
- Kizer, K.O., Phatnani, H.P., Shibata, Y., Hall, H., Greenleaf, A.L., and Strahl, B.D. (2005). A novel domain in Set2 mediates RNA polymerase II interaction and couples histone H3 K36 methylation with transcript elongation. *Mol. Cell. Biol.* **25**, 3305–3316.
- Kobayashi, S., Boggon, T.J., Dayaram, T., Janne, P.A., Kocher, O., Meyerson, M., Johnson, B.E., Eck, M.J., Tenen, D.G., and Halmos, B. (2005). EGFR mutation and resistance of non-small-cell lung cancer to gefitinib. *N. Engl. J. Med.* **352**, 786–792.
- Koike-Yusa, H., Li, Y., Tan, E.P., Velasco-Herrera, Mdel.C., and Yusa, K. (2014). Genome-wide recessive genetic screening in mammalian cells with a lentiviral CRISPR-guide RNA library. *Nat. Biotechnol.* **32**, 267–273.
- Kwiatkowski, N., Zhang, T., Rahl, P.B., Abraham, B.J., Reddy, J., Ficarro, S.B., Dastur, A., Amzallag, A., Ramaswamy, S., Tesar, B., et al. (2014). Targeting transcription regulation in cancer with a covalent CDK7 inhibitor. *Nature* **511**, 616–620.
- Ledermann, J.A., Harter, P., Gourley, C., Friedlander, M., Vergote, I., Rustin, G., Scott, C., Meier, W., Shapira-Frommer, R., Safra, T., et al. (2016). Overall survival in patients with platinum-sensitive recurrent serous ovarian cancer receiving olaparib maintenance monotherapy: an updated analysis from a randomised, placebo-controlled, double-blind, phase 2 trial. *Lancet Oncol.* **17**, 1579–1589.
- McBride, J.L., Boudreau, R.L., Harper, S.Q., Staber, P.D., Monteys, A.M., Martins, I., Gilmore, B.L., Burstein, H., Peluso, R.W., Polisky, B., et al. (2008). Artificial miRNAs mitigate shRNA-mediated toxicity in the brain: implications for the therapeutic development of RNAi. *Proc. Natl. Acad. Sci. U S A* **105**, 5868–5873.
- Meacham, C.E., Ho, E.E., Dubrovsky, E., Gertler, F.B., and Hemann, M.T. (2009). In vivo RNAi screening identifies regulators of actin dynamics as key determinants of lymphoma progression. *Nat. Genet.* **41**, 1133–1137.
- Mullighan, C.G., Zhang, J., Kasper, L.H., Lerach, S., Payne-Turner, D., Phillips, L.A., Heatley, S.L., Holmfeldt, L., Collins-Underwood, J.R., Ma, J., et al. (2011). CREBBP mutations in relapsed acute lymphoblastic leukaemia. *Nature* **471**, 235–239.
- Ng, K.P., Hillmer, A.M., Chuah, C.T.H., Juan, W.C., Ko, T.K., Teo, A.S.M., Ariyaratne, P.N., Takahashi, N., Sawada, K., Fei, Y., et al. (2012). A common BIM deletion polymorphism mediates intrinsic resistance and inferior responses to tyrosine kinase inhibitors in cancer. *Nat. Med.* **18**, 521–528.

- O'Leary, B., Finn, R.S., and Turner, N.C. (2016). Treating cancer with selective CDK4/6 inhibitors. *Nat. Rev. Clin. Oncol.* *13*, 417–430.
- Pao, W., Miller, V.A., Politi, K.A., Riely, G.J., Somwar, R., Zakowski, M.F., Kris, M.G., and Varmus, H. (2005). Acquired resistance of lung adenocarcinomas to gefitinib or erlotinib is associated with a second mutation in the EGFR kinase domain. *PLoS Med.* *2*, e73.
- Peña-Llopis, S., Vega-Rubín-de-Celis, S., Liao, A., Leng, N., Pavia-Jiménez, A., Wang, S., Yamasaki, T., Zhrebker, L., Sivanand, S., Spence, P., et al. (2012). BAP1 loss defines a new class of renal cell carcinoma. *Nat. Genet.* *44*, 751–759.
- Prasad, V. (2016). Perspective: the precision-oncology illusion. *Nature* *537*, S63.
- Pritchard, J.R., Bruno, P.M., Gilbert, L.A., Capron, K.L., Lauffenburger, D.A., and Hemann, M.T. (2013). Defining principles of combination drug mechanisms of action. *Proc. Natl. Acad. Sci. U S A* *110*, E170–E179.
- Robson, M., Im, S.-A., Senkus, E., Xu, B., Domchek, S.M., Masuda, N., Delaloge, S., Li, W., Tung, N., Armstrong, A., et al. (2017). Olaparib for metastatic breast cancer in patients with a germline BRCA mutation. *N. Engl. J. Med.* *377*, 523–533.
- Rogers, Z.N., McFarland, C.D., Winters, I.P., Naranjo, S., Chuang, C.-H., Petrov, D., and Winslow, M.M. (2017). A quantitative and multiplexed approach to uncover the fitness landscape of tumor suppression in vivo. *Nat. Methods* *14*, 737–742.
- Shaffer, S.M., Dunagin, M.C., Torborg, S.R., Torre, E.A., Emert, B., Krepler, C., Beqiri, M., Sproesser, K., Brafford, P.A., Xiao, M., et al. (2017). Rare cell variability and drug-induced reprogramming as a mode of cancer drug resistance. *Nature* *546*, 431–435.
- Shalem, O., Sanjana, N.E., Hartenian, E., Shi, X., Scott, D.A., Mikkelsen, T., Heckl, D., Ebert, B.L., Root, D.E., Doench, J.G., and Zhang, F. (2014). Genome-scale CRISPR-Cas9 knockout screening in human cells. *Science* *343*, 84–87.
- Sos, M.L., Koker, M., Weir, B.A., Heynck, S., Rabinovsky, R., Zander, T., Seeger, J.M., Weiss, J., Fischer, F., Frommolt, P., et al. (2009). PTEN loss contributes to erlotinib resistance in EGFR-mutant lung cancer by activation of Akt and EGFR. *Cancer Res.* *69*, 3256–3261.
- Stauffer, D., Chang, B., Huang, J., Dunn, A., and Thayer, M. (2007). p300/CREB-binding protein interacts with ATR and is required for the DNA replication checkpoint. *J. Biol. Chem.* *282*, 9678–9687.
- Takase, S., Kurokawa, R., Arai, D., Kanemoto Kanto, K., Okino, T., Nakao, Y., Kushiro, T., Yoshida, M., and Matsumoto, K. (2017). A quantitative shRNA screen identifies ATP1A1 as a gene that regulates cytotoxicity by aurilide B. *Sci. Rep.* *7*, 2002.
- Tan, D.S.P., Rothermundt, C., Thomas, K., Bancroft, E., Eeles, R., Shanley, S., Ardern-Jones, A., Norman, A., Kaye, S.B., and Gore, M.E. (2008). “BRCAness” syndrome in ovarian cancer: a case-control study describing the clinical features and outcome of patients with epithelial ovarian cancer associated with BRCA1 and BRCA2 mutations. *J. Clin. Oncol.* *26*, 5530–5536.
- Testa, J.R., Cheung, M., Pei, J., Below, J.E., Tan, Y., Sementino, E., Cox, N.J., Dogan, A.U., Pass, H.I., Trusa, S., et al. (2011). Germline BAP1 mutations predispose to malignant mesothelioma. *Nat. Genet.* *43*, 1022–1025.
- Thomson, S., Buck, E., Petti, F., Griffin, G., Brown, E., Ramnarine, N., Iwata, K.K., Gibson, N., and Haley, J.D. (2005). Epithelial to mesenchymal transition is a determinant of sensitivity of non-small-cell lung carcinoma cell lines and xenografts to epidermal growth factor receptor inhibition. *Cancer Res.* *65*, 9455–9462.
- Tutt, A., Robson, M., Garber, J.E., Domchek, S.M., Audeh, M.W., Weitzel, J.N., Friedlander, M., Arun, B., Loman, N., Schmutzler, R.K., et al. (2010). Oral poly(ADP-ribose) polymerase inhibitor olaparib in patients with BRCA1 or BRCA2 mutations and advanced breast cancer: a proof-of-concept trial. *Lancet* *376*, 235–244.
- Unno, J., Itaya, A., Taoka, M., Sato, K., Tomida, J., Sakai, W., Sugawara, K., Ishiai, M., Ikura, T., Isobe, T., et al. (2014). FANCD2 binds CtIP and regulates DNA-end resection during DNA interstrand crosslink repair. *Cell Rep.* *7*, 1039–1047.
- Vassilev, L.T., Vu, B.T., Graves, B., Carvajal, D., Podlaski, F., Filipovic, Z., Kong, N., Kammlott, U., Lukacs, C., Klein, C., et al. (2004). In vivo activation of the p53 pathway by small-molecule antagonists of MDM2. *Science* *303*, 844–848.
- Viswanathan, V.S., Ryan, M.J., Dhruv, H.D., Gill, S., Eichhoff, O.M., Seashore-Ludlow, B., Kaffenberger, S.D., Eaton, J.K., Shimada, K., Aguirre, A.J., et al. (2017). Dependency of a therapy-resistant state of cancer cells on a lipid peroxidase pathway. *Nature* *547*, 453–457.
- Wang, T., Wei, J.J., Sabatini, D.M., and Lander, E.S. (2014). Genetic screens in human cells using the CRISPR-Cas9 system. *Science* *343*, 80–84.
- Weinstein, J.N., and Lorenzi, P.L. (2013). Cancer: discrepancies in drug sensitivity. *Nature* *504*, 381–383.
- Williams, R.T., Roussel, M.F., and Sherr, C.J. (2006). Arf gene loss enhances oncogenicity and limits imatinib response in mouse models of Bcr-Abl-induced acute lymphoblastic leukemia. *Proc. Natl. Acad. Sci. U S A* *103*, 6688–6693.
- Yang, W., Soares, J., Greninger, P., Edelman, E.J., Lightfoot, H., Forbes, S., Bindal, N., Beare, D., Smith, J.A., Thompson, I.R., et al. (2013). Genomics of Drug Sensitivity in Cancer (GDSC): a resource for therapeutic biomarker discovery in cancer cells. *Nucleic Acids Res.* *41*, D955–D961.
- Yauch, R.L., Januario, T., Eberhard, D.A., Cavet, G., Zhu, W., Fu, L., Pham, T.Q., Soriano, R., Stinson, J., Seshagiri, S., et al. (2005). Epithelial versus mesenchymal phenotype determines in vitro sensitivity and predicts clinical activity of erlotinib in lung cancer patients. *Clin. Cancer Res.* *11*, 8686–8698.
- Yu, H., Pak, H., Hammond-Martel, I., Ghram, M., Rodrigue, A., Daou, S., Barbour, H., Corbeil, L., Hébert, J., Drobetsky, E., et al. (2014). Tumor suppressor and deubiquitinase BAP1 promotes DNA double-strand break repair. *Proc. Natl. Acad. Sci. U S A* *111*, 285–290.
- Yuan, H., Li, N., Fu, D., Ren, J., Hui, J., Peng, J., Liu, Y., Qiu, T., Jiang, M., Pan, Q., et al. (2017). Histone methyltransferase SETD2 modulates alternative splicing to inhibit intestinal tumorigenesis. *J. Clin. Invest.* *127*, 3375–3391.
- Zhu, S., Cao, Z., Liu, Z., He, Y., Wang, Y., Yuan, P., Li, W., Tian, F., Bao, Y., and Wei, W. (2019). Guide RNAs with embedded barcodes boost CRISPR-pooled screens. *Genome Biol.* *20*, 20.

## STAR★METHODS

### KEY RESOURCES TABLE

REAGENT or RESOURCE	SOURCE	IDENTIFIER
<b>Antibodies</b>		
$\gamma$ -H2AX-Ser139	Millipore	Cat#05-636; RRID:AB_309864
BAP1	Santa Cruz	Cat#SC-28383; RRID:AB_626723
DNMT1	Abcam	Cat#ab13537; RRID:AB_300438
PARP	Cell signaling Technologies	Cat#9542; RRID:AB_2160739
FLAG	Abmart	Cat#M20008; RRID:AB_2713960
Myc	Abmart	Cat#M20002
HA	Abmart	Cat#M20003
SETD2	Abclonal	Cat#A3194; RRID:AB_2764980
Fibrillarin	Abcam	Cat#ab5821; RRID:AB_2105785
Coilin	Abcam	Cat#ab87913; RRID:AB_10860831
CREBBP	Abcam	Cat#ab2832; RRID:AB_303342
CDH1	BD Bioscience	Cat#610181; RRID:AB_397580
VIM	Cell signaling Technologies	Cat#5741; RRID:AB_10695459
EGFR	Cell signaling Technologies	Cat#4267; RRID:AB_2246311
EGFR Y1058	Cell signaling Technologies	Cat#3777; RRID:AB_2096270
S6K pT389	Cell signaling Technologies	Cat#9205; RRID:AB_330944
S6K	Cell signaling Technologies	Cat#9202; RRID:AB_331676
AKT pS473	Cell signaling Technologies	Cat#4060; RRID:AB_2315049
AKT pT308	Cell signaling Technologies	Cat#13038; RRID:AB_2629447
BIM	Cell signaling Technologies	Cat#2933; RRID:AB_1030947
Actin	Cell signaling Technologies	Cat#4967; RRID:AB_330288
Alexa 647 Goat anti Mouse	Sigma	Cat#50185; RRID:AB_1137661
Alexa 647 Goat anti Rabbit	Sigma	Cat#40839; RRID:AB_1137669
<b>Bacterial and Virus Strains</b>		
<i>E. coli</i> stable competent (high efficiency)	Transgene	Cat#CD201
<b>Chemicals, Peptides, and Recombinant Proteins</b>		
Polybrene	Sigma-Aldrich	Cat#H9268
Puromycin	Gold Biotechnology	Cat#P-600-500
TRIzol	Life Technologies	Cat#15596018
RNase A	Thermo Fisher Scientific	Cat#EN0531
Doxorubicin	Selleck	Cat#S1208
Camptothecin	Selleck	Cat#S1288
Cisplatin	Selleck	Cat#S1166
Mitomycin C	Selleck	Cat#S8146
Fluorouracil	Selleck	Cat#S1209
Gemcitabine	Selleck	Cat#S1714
Methotrexate	Selleck	Cat#S1210
Thioguanine	Selleck	Cat#S1774
Cytarabine	Selleck	Cat#S1648
Paclitaxel	Selleck	Cat#S1150
Vincristine	Selleck	Cat#S1241
Actinomycin D	MCE	Cat#HY-17559
Arsenic trioxide	A gift from Yajie Wang	N/A

(Continued on next page)

**Continued**

REAGENT or RESOURCE	SOURCE	IDENTIFIER
Decitabine	Selleck	Cat#S1200
Vorinostat	Selleck	Cat#S1047
Palbociclib	Selleck	Cat#S1579
Tanespimycin	Selleck	Cat#S1141
Torkinib	Selleck	Cat#S2218
Erlotinib	Selleck	Cat#S1023
PI-103	Selleck	Cat#S1038
MK2206	Selleck	Cat#S1078
Olaparib	Selleck	Cat#S1060
Apabetalone	Selleck	Cat#S7295
(+)-JQ1	Selleck	Cat#S7110
THZ1	Selleck	Cat#S7549
EPZ005687	Selleck	Cat#S7004
Immobilon Western HRP substrate	Millipore	Cat# WBKLS0500
Propidium Iodide	Sigma	Cat#P4170
PMSF	Beyotime	Cat#ST506
FLAG M2 Agarose	Sigma	Cat#A2220
MYC Agarose	Biotoools	Cat#B23401
FLAG peptide	Biotoools	Cat#B23111
MYC peptide	Biotoools	Cat#B23411
Protein A/G Plus Agarose	Thermo Fisher	Cat#20423
Critical Commercial Assays		
GoTaq® qPCR and RT-qPCR Systems	Promega	Cat#A6001
GoScript Reverse Transcription System	Promega	Cat#A5001
Deposited Data		
Data points for <a href="#">Figure 1D</a> are provided in <a href="#">Data S1</a>	This paper	N/A
Experimental Models: Cell Lines		
Human Cell line:786O	Cell Bank, China Academy of Sciences	Cat#TCHu186
Human Cell line:769P	Cell Bank, China Academy of Sciences	Cat#TCHu215
Human Cell line:OSRC2	Cell Bank, China Academy of Sciences	Cat#TCHu40
Human Cell line:PC9	A gift from Hongbin Ji	N/A
Human Cell line:UM-UC-3	Cell Bank, China Academy of Sciences	Cat#TCHu217
Mouse cell line:Eu-Myc p19 <sup>Arf</sup> <sup>-/-</sup> cell	A gift from Michael Hemann	N/A
Mouse cell line:ALL	A gift from Michael Hemann	N/A
Human Cell line:Phoenix	A gift from Michael Hemann	N/A
Human Cell line:293T	Cell Bank, China Academy of Sciences	Cat#GNHu17
Experimental Models: Organisms/Strains		
BALB/c nude mice	Shanghai SLRC laboratory	N/A
Oligonucleotides		
shRNA See <a href="#">Data S2</a>	This paper	N/A
qRT-PCR primers See <a href="#">Data S2</a>	This paper	N/A
Recombinant DNA		
pMSCV-IRES-GFP	A gift from Michael Hemann	N/A
pSi	A gift from Michael Hemann	N/A
pBABE	A gift from Hongbin Ji	N/A
pcDNA3.1-N-FLAG-BAP1	This paper	N/A
pcDNA3.1-N-FLAG	This paper	N/A

(Continued on next page)

**Continued**

REAGENT or RESOURCE	SOURCE	IDENTIFIER
pcDNA3.1-MYC	This paper	N/A
pcDNA3.1-N-FLAG-CBX1	This paper	N/A
pcDNA3.1-MYC-CBX1	This paper	N/A
pcDNA3.1-MYC-DNMT1	This paper	N/A
Software and Algorithms		
shRNA Design	Hemann Lab shRNA Database	<a href="http://euphrates.mit.edu/cgi-bin/shRNA/index.pl">http://euphrates.mit.edu/cgi-bin/shRNA/index.pl</a>
GraphPad Prism 7	GraphPad Software	<a href="https://www.graphpad.com/">https://www.graphpad.com/</a>
ImageJ	NIH	<a href="https://imagej.nih.gov/ij/">https://imagej.nih.gov/ij/</a>
SPSS 20.0	SPSS	<a href="https://www.ibm.com/cn-zh/analytics/spss-statistics-software">https://www.ibm.com/cn-zh/analytics/spss-statistics-software</a>
Flowjo	Flowjo	<a href="https://www.flowjo.com/">https://www.flowjo.com/</a>
LAS AF Lite	Leica	<a href="https://www.leica-microsystems.com/">https://www.leica-microsystems.com/</a>
Snapgene	Snapgene	<a href="https://www.snapgene.com/">https://www.snapgene.com/</a>
Other		
RPMI 1640 Medium	HyClone	Cat#SH30809.01
DMEM Medium	HyClone	Cat#SH30243.01
Trypsin-EDTA 0.25%	GIBCO	Cat#25200-056
Pen Strep	GIBCO	Cat#15140-122
Fetal bovine serum	GIBCO	Cat#10091-148
PBS	HyClone	Cat#SH30013.03
IMDM Medium	HyClone	Cat#SH30228.01
PVDF membrane	Millipore	Cat#IPVH00010

**CONTACT FOR REAGENT AND RESOURCE SHARING**

Further information and requests for resources and reagents should be directed to and will be fulfilled by the Lead Contact, Hai Jiang ([hai@sibcb.ac.cn](mailto:hai@sibcb.ac.cn)).

**EXPERIMENTAL MODEL AND SUBJECT DETAILS****Cell lines**

E $\mu$ -Myc p19<sup>Arf</sup> <sup>-/-</sup> cell (sex: male) was cultured in B cell medium (45% Dulbecco's modified Eagle's medium and 45% Iscove's modified Dulbecco's media, supplemented with 10% fetal bovine serum, L-glutamate, and 5  $\mu$ M  $\beta$ -mercaptoethanol). BCR-ABL ALL cell (generated in (Williams et al., 2006), sex unknown) was cultured in RPMI medium supplemented with 10% fetal bovine serum, L-glutamate, and 5  $\mu$ M  $\beta$ -mercaptoethanol). Phoenix (sex: female), HEK293T (sex: female) and UM-UC-3 cells (sex: male) were cultured in DMEM medium supplemented with L-glutamate and 10% fetal bovine serum. PC-9 (sex: male), 786-O (sex: male), 769-P (sex: female), OS-RC-2 (sex: male) were cultured in RPMI 1640 medium supplemented with 10% fetal bovine serum and 100 U/mL penicillin/streptomycin at 37°C with 5% CO<sub>2</sub>.

**E $\mu$ -Myc p19<sup>Arf</sup> <sup>-/-</sup> Cell line maintenance**

Commonly used cancer cell lines undergo genetic diversification mainly due to genomic instability. More than half of human cancers inactivate p53, which guard genome from acquiring mutations and aneuploidy. In addition, mutations in the wide spectrum of genes involved in DNA damage response, such as BRCA1/2, ATM, etc., also affect the genomic stabilities of many human cancer cell lines. As for the E $\mu$ -Myc p19<sup>Arf</sup> <sup>-/-</sup> cells, it was first established in Scott Lowe lab, and served as a good performing platform in research and screening field (Bric et al., 2009; Bruno et al., 2017; Burgess et al., 2008; Dickins et al., 2005; Jiang et al., 2011; Meacham et al., 2009). The modifications in its genome are E $\mu$  enhancer-driven Myc overexpression and Arf knockout. p53 and DNA repair pathways are left untouched in this situation, which will guard against rapid genomic diversification. It can be seen from Figure 1D that knockdown of p53 and DNA repair pathway components such as BRCA1/2, ATM, BLM, NBS1, WRN etc. each produced expected resistance or sensitization phenotypes, which attests that p53 and major DNA repair pathways remain functional in this cell line. This will guard against rapid genetic diversification.

In experimental protocols, we also take additional cautions to avoid genomic and transcriptional diversifications in the experimental system. To avoid sub-clone effect, large amount of early-passage E $\mu$ -Myc p19<sup>Arf-/-</sup> cells were frozen in separate vials, and cells were discarded if they have been in culture for more than 40 days.

### Mice

5-6-wk-old female nude mice were used for all experiments. BALB/c nude mice were purchased from Shanghai SLRC laboratory. Prior to all experiments, purchased mice were allowed one week to acclimate to housing conditions at the Shanghai Institute of Biochemistry and Cell Biology Animal Facility. All experimental mice were housed in specific SPF conditions and used in accordance with animal care guidelines from the Shanghai Institute of Biochemistry and Cell Biology Animal Welfare and Ethical Review committee. Animal protocols were approved by the Shanghai Institute of Biochemistry and Cell Biology Animal Welfare and Ethical Review committee.

## METHOD DETAILS

### GFP-based cell survival competition assay to determine sensitivity change caused by tumor suppressor loss

The experimental protocol of this assay has been previously described (Bruno et al., 2017; Jiang et al., 2011; Pritchard et al., 2013). The E $\mu$ -Myc p19<sup>Arf-/-</sup> cell line was chosen as the initial experimental system partly because as a genetically engineered cancer cell line, it contains low level of mutations, making it suitable for interrogating gene-drug interactions in a systematic manner. Previous studies (Jiang et al., 2011) also demonstrated that in this cell line drug sensitivity change can be reliably analyzed. Briefly,  $1 \times 10^5$  E $\mu$ -Myc p19<sup>Arf-/-</sup> cells are infected with retrovirus that express GFP and shRNA targeting a tumor suppressor gene. Retrovirus is diluted so that infection rate, as judged by GFP positivity, is around 20%–40%. Cells are counted and seeded at 1 million cells per 1 ml in 48-well plates and treated with various drugs at lethal dose 80 to 90 (LD80-90). Half of the volume from each experiment is removed and replenished with fresh medium every 24 hr. Cells are analyzed by fluorescence-activated cell sorting (FACS), with propidium iodide as a viability marker. LD80-90 of drugs are concentrations at which, when used to treat uninfected E $\mu$ -Myc p19<sup>Arf-/-</sup> cells, cause death in 80%–90% of cells.

At 72 hr, treated and untreated cells are analyzed by flow cytometry. The drug-treated samples contain at least 50,000 live cells at 72 hr. Around 1,000 live cells are analyzed to determine the percentage of GFP-expression cells, which are then used to calculate relative resistance index. To avoid outgrowth of untreated control cells, we typically seeded them at 0.25 million per ml, and 75% of medium was replaced at 24 hr and 48 hr.

### Calculation of relative resistance/sensitivity from GFP-based cell survival competition assay

In our assay, the change of drug sensitivity caused by an shRNA will influence the percentage of GFP-positive, shRNA expressing cells in surviving population. The GFP percentage with and without drug treatment can be used to calculate relative resistance index based on methods as previously described (Jiang et al., 2011).

Briefly, to compare the extent of drug sensitivity change conferred by gene knockdown, we introduce the concept of RI (relative resistance index). We define the value of RI as X. The biological meaning of this factor X is that when a mixture of uninfected (GFP-negative) and infected (GFP-positive & gene knockdown) cells are treated with a drug, the infected (knockdown) cells will be X-fold as likely to survive drug treatment when compared to uninfected cells. By this definition, if one out of N uninfected cells survives a drug treatment, then X out of N infected cells should survive. If we define the total number of uninfected and infected cells as T and the GFP percentage of untreated population as G1, then after drug treatment, the number of surviving, uninfected cells (N-un) can be calculated as  $N-un = T \times (1 - G1) \times 1/N$ , and the number of surviving, infected cells (N-in) can be calculated as  $N-in = T \times G1 \times X/N$ . Therefore, the GFP percentage of the treated, surviving population (G2) can be calculated as  $G2 = (N-in)/(N-un + N-in)$ . From this equation, it can be derived that  $X = (G2 - G1 \times G2)/(G1 - G1 \times G2)$ . Such an equation was used to compute RI values for each shRNA-drug pair.

For example, if a gene knockdown confers resistance to a drug, the GFP percentage in surviving cells may increase from 20% (G1) to 50% (G2) after drug treatment. Therefore, for cells with gene knockdown, the relative resistance index (RI)  $X = (0.5 - 0.5 \times 0.2)/(0.2 - 0.5 \times 0.2) = 4$ , meaning that cells with gene knockdown are 4-fold as likely to survive drug treatment, compared to control cells.

If a gene knockdown sensitizes cells to a drug, then GFP percentage after treatment will decrease. In this case, the relative resistance index will be smaller than 1. For example, a relative resistance index (X) of 0.1 means knockdown cells are 0.1-fold as likely to survive drug treatment compared to control cells. In other words, gene knockdown made cells 10-fold as sensitive to a drug compared to control cells. To more clearly represent this sensitization effect in a heatmap, a conversion is used in Figure 1D. A relative resistance index of 0.1 is converted to a sensitivity fold of  $-10$ . A relative resistance index of 0.2 is converted to a sensitivity fold of  $-5$  and so on. The intact dataset of all the shRNA and drugs was shown in Data S1.

### Cell line comparison-based data acquisition

On the GDSC website, gene-drug relationship is acquired through <https://www.cancerrxgene.org/translation/Feature>. Established cancer genes such as p53, BRCA1 are listed there. The effect size is proportional to the difference in mean IC<sub>50</sub> between wild-type and mutant cell lines. Numbers less than 0 indicate drug sensitivity, numbers greater than 0 indicate drug resistance. For

example, p value ranked p53-drug interactions can be accessed at <https://www.cancerrxgene.org/translation/Feature/289>, effect size > 0 means mutation of p53 leads to resistance to a drug, and effect size < 0 means mutation of p53 leads to sensitivity to a drug. All tumor suppressor genes listed in the GDSC webpage were checked as of August 2018 and all gene-drug interactions whose p value are lower than 0.001 and false discovery rate are lower than 10% were documented in Table S1. Tables S2 and S3 listed tumor suppressor-drug interactions that have been validated in clinical observations. BRCA1/2 loss causes enhanced sensitivity to DNA damage drug and PARP inhibitor. Table S2 showed how the GDSC data predict BRCA1/2 mutations would affect cellular sensitivity to cisplatin and PARP inhibitors. Similar approaches were used to generate Table S3.

### Constructs

Retroviral pMSCV-IRES-GFP vector was kindly provided by Professor Michael Hemann at MIT and was used to set up mouse and human retro shRNA system. Compared with commonly used pLKO.1 shRNA vector, this mir-30-based shRNA vector are less prone to cause off-target effects and toxic immune response to host cells (Fellmann et al., 2013). The cloning procedure was performed as described (Jiang et al., 2011). Multiple shRNAs were cloned for each gene, and 5 to 6 shRNAs were tested. Real-time PCR was performed to confirm gene knockdown efficiency. Presentation of drugs sensitivity was based on three shRNAs that effectively knock-down target genes. In Figure 1D we presented drug sensitivity changes when all three shRNAs caused drug resistance, or when all three shRNAs caused drug sensitization. Average resistance or sensitivity scores from these shRNAs were presented in Figure 1D. In addition, when carrying out our experiments, if a shRNA construct causes unfitness in cells (which can be easily monitored by reduction of the percentage of GFP positive in shRNA-expressing cells), such shRNA constructs were not used for further analysis. Unfitness can be caused either by interfering with genes vital to E $\mu$ -Myc p19<sup>Arf</sup><sup>-/-</sup> cells (Data S2), or by causing immune, toxic response to host cells. With such measures we further limited the effect of potential immune response triggered by RNAi.

All shRNA sequences used in this study are listed in Data S2.

Human KRAS G12V was cloned into pBABE retroviral expression vector.

### Cell cycle analyses

After treated with drugs for 24hr, cells were collected and fixed overnight in 70% ethanol. Cells were then treated with 0.2% Triton X-100, 50  $\mu$ g/ml propidium iodide and 100  $\mu$ g/ml RNase A for 40 min and analyzed by FACS.

### Western Blot and Immunoprecipitation

Cells in culture were washed with ice-cold PBS twice to completely remove residual medium before resuspension in PBS. 2xSDS lysis buffer (30% Glycerol, 5%  $\beta$ -mercaptoethanol, 0.02% bromophenol blue, 10% SDS and 250mM TrisHCl pH 6.8) was directly added to resuspended cells. Cell lysates were boiled at 100°C for 10 min. Equal volume and equal quantity of protein samples were subjected to SDS-PAGE and transferred to a PVDF membrane (Millipore, cat# WBKLS0500). The membrane was blocked in 5% milk at room temperature for 1hr and incubated with appropriate antibodies at 4°C overnight. On the next day, the membrane was washed with TBS-T three times and incubated with appropriate secondary HRP antibodies in 5% BSA at room temperature for 1hr. The membrane was washed again with TBS-T three times and ECL was applied for film development.

For immunoprecipitation experiments, equal amounts of whole cell extracts (WCEs) were incubated with anti-Flag/MYC at 4°C for overnight and then with proteinA/G Agarose beads at 4°C for 2 hours. The beads were washed with cell lysis buffer at 4°C three times, boiled in 2xSDS buffer, and then frozen until use.

### Immunofluorescence staining

769-P cells were fixed after 24hr treatment with THZ1. Cells were then fixed and stained with anti-Fibrillarin (Abcam, #ab5821, 1:400), anti-Coilin (Abcam, #ab87913, 1:200) and DAPI. Alexa 647-anti rabbit used as a secondary antibody. A Leica TCS SP8 microscope was used for imaging. Image analysis was performed using LAS AF Lite on the original images. Cell counts and fluorescence normalization were generated ImageJ software.

### Colony formation assay

5000 cells were resuspended in medium containing 10% FBS and plated in 6-well plates. After 24hr, they were treated with the indicated dose of drugs. After 24hr or 12hr of treatment, drug-containing medium was replaced with fresh complete culture medium and cell colonies were allowed to grow for about 10 days. Colonies were then fixed with 4% paraformaldehyde and stained with 0.1% crystal violet for 30 min. Stained cell colonies were washed with phosphate buffered saline (PBS) for three times and dried. Images were obtained by a digital camera. Colony formation assay were repeated in three independent experiments, and the figures showed representative images.

### RNA extraction and qRT-PCR

RNA was isolated from 10<sup>6</sup> cells using Trizol extraction. For qRT-PCR, RNA samples were reversely transcribed into cDNA using the GoScript Reverse Transcript System (Promega). cDNA samples were then subjected to qRT-PCR quantification in duplicate on a Biorad CFX Connect Real Time machine.

### Ubiquitination assay

HEK293T cells transfected with FLAG-BAP1, MYC-DNMT1 and HA-UB plasmid were treated with 20  $\mu\text{mol/L}$  of MG132, a proteasome inhibitor for 6hr. Cell lysate protein was used for immunoprecipitation with anti-MYC agarose. After washing, immunoprecipitates were resolved by SDS-PAGE and proteins transferred onto PVDF membranes. Ubiquitinated DNMT1 was detected by western blotting using anti-HA antibody.

### Generation of nude mice xenografts and drug treatment

Six-week-old male nude mice with BALB/c genetic background were used in the experiments. All mice were housed in a pathogen-free environment at Shanghai Institute of Biochemistry and Cell Biology and treated in strictly accordance with protocols approved by the Institutional Animal Care and Use Committee of the Shanghai Institute of Biochemistry and Cell Biology, Chinese Academy of Sciences. One million OS-RC-2 or PC-9 cells were injected s.c. into the flanks of mice in 100  $\mu\text{L}$  PBS. 8 days for OS-RC-2 or 10 days for PC-9 after injection, THZ1 in D5W (5 mg/kg body weight, intraperitoneally, once a day) or erlotinib in 1% Tween-80 (16 mg/kg body weight, intragastrical, once a day), or irinotecan in 1% Tween-80 (50 mg/kg body weight, intraperitoneally, every four days) was administered. Control animals received D5W or 1% Tween-80 as vehicle. For PC-9 cells, tumor growth was monitored for 24 days and the tumors were measured with a caliper every 2 days; for OS-RC-2 cells, tumor growth was monitored for 28 days and the tumors were measured with a caliper every 5 days. Tumor volume was calculated as  $0.5 \times L \times W \times W$ , and the tumors were weighed, processed, and imaged after surgical removal.

### Kaplan-Meier survival curve

Kaplan-Meier curve for risk groups, concordance index (CI), and p value of the log-rank testing equality of survival curves was constructed using samples of TCGA LUSC datasets by SurvExpress program (Aguirre-Gamboa et al., 2013). Red and black curves denote High- and Low-risk groups respectively. The y axis indicates the percentage of survival, the x axis represents survival days, and the number of survivors at the corresponding time. Censoring samples are shown as “+” marks. The number of individuals, the number of censored, and the CI of each risk group are shown in the top-right insets. The CI (concordance index) estimated the probability that subjects with a higher risk (in this case CREBBP-high expression) will die before subjects with a lower risk (CREBBP-low expression), which indicating the reliability of calculated model. The concordance index will equal 0.5 for randomly selected pairs.

### QUANTIFICATION AND STATISTICAL ANALYSIS

Differences of event frequency between two groups were analyzed using Student's unpaired two-tailed t test after testing the equality of variances. For individual samples of large population, Kolmogorov-Smirnov normality test were performed ahead of t test. For *in vivo* experiments, due to the small number of samples Wilcoxon test were used. All analysis used using Prism 7 (GraphPad). A p value > 0.05 was considered not significant, and p values < 0.001 were marked as \*\*\* in figures, p values < 0.01 were marked as \*\* in figures and p values < 0.05 were marked as \* in figures.

### DATA AND SOFTWARE AVAILABILITY

Data points for Figure 1D are provided in Data S1.